SIMULATION OF VENUS-LIKE CANDIDATE ATMOSPHERES TO REFINE THE FUTURE UNDERSTANDING OF TERRESTRIAL EXOPLANET CHARACTERISATION

A Thesis submitted by

Emma Miles (BSc USQ)

Student ID: [redacted]

For the award of

Bachelor of Science (Honours)

September 2022

ABSTRACT

Astronomical research is strongly focused on the search for terrestrial exoplanets. One of the ways to determine if an exoplanet is terrestrial, is through the characterisation of its atmosphere. This project focuses on the characterisation of the atmospheres of exoplanets with similar astrophysical parameters to Venus, a terrestrial planet in our solar system, to guide the direction of the observations for the next generation of space-based observatories. the Python programs, PLATON and TauREx, are used to simulate and model the atmospheres of Venus-like candidates which were identified using the NASA Exoplanet Archive. Four exoplanets, TRAPPIST-1b, TRAPPIST-1c, GJ 9827c and Kepler 138c, are modelled and compared to the ancient Venus atmospheric model to establish any similarities and differences. Similarities were found between the molecular species present in the atmospheres of ancient Venus, TRAPPIST-1b, TRAPPIST-1c and Kepler 138c. However, the differences found with the atmosphere of GJ 9827c suggest that it is a gaseous exoplanet. Given the limitations of the simulations and models produced here, the hypothesis should be explored further. The simulated wavelengths determined in these models are likely to be detectable by the instruments of the James Webb Space Telescope (JWST) and other future space-based missions. The models are expected to refine the classification of terrestrial exoplanets, and expand our knowledge of planetary system evolution.

CERTIFICATION OF THESIS

I Emma Miles, declare that this Thesis entitled *SIMULATION OF VENUS-LIKE CANDIDATE ATMOSPHERES TO REFINE THE FUTURE UNDERSTANDING OF TERRESTRIAL EXOPLANET CHARACTERISATION* contains no material that has been submitted previously, in whole or in part, for the award of any other academic degree or diploma. Except where otherwise indicated, this thesis is my own work.

Signed: Date:

Endorsed by:

Dr Carolyn Brown
Principal Supervisor

Student and supervisors' signatures of endorsement are held at the University.

ACKNOWLEDGEMENTS

I would like to sincerely thank my family and friends, especially my parents, Phim and Michael, my brother, Aaron, and my partner, Vasko, who all greatly supported me throughout my Honours project. I would also like to express my deepest gratitude to Tim, Rocko, and Luna for their emotional (and technical) support. Without you, my Honours would not have been possible.

Pictured: *Honours Technical (and emotional) Support Crew (Circa 2022).*

A special thank you to PhD Candidate Nataliea Lowson for her assistance with using TauREx, as well as Dr George Zhou and Associate Professor Duncan Wright for their guidance throughout my Honours project. I would also like to extend my sincere thanks to Dr Joanna Turner, for going above and beyond to support me throughout my Honours, and Richard Young, for his technical assistance with the HPC (even

though I wasn't able to use it in this project… sorry). Thank you to Professor Brad Carter and the Centre of Astrophysics for their financial support.

And finally, I would like to express my deepest appreciation to my supervisor, Dr Carolyn Brown, who offered encouragement and advice (along with insight and humour) throughout my Honours. Your guidance and wisdom helped me through this journey, and I am forever grateful.

This research has made use of NASA's Astrophysics Data System Bibliographic Services and the NASA Exoplanet Archive, which is operated by the California Institute of Technology, under contract with the National Aeronautics and Space Administration under the Exoplanet Exploration Program.

TABLE OF CONTENTS

LIST OF TABLES

LIST OF FIGURES

CHAPTER 1: INTRODUCTION

In the past, the possibility of life existing beyond Earth was something exclusive to science fiction. As the technology for astronomical research advances and preparations for future missions begin, such as the collection of data from the James Webb Space Telescope (JWST), finding a habitable planet beyond our Solar System is likely to become a reality.

Current astronomical research is strongly focused on the search for exoplanets, specifically planetary systems likely to contain terrestrial exoplanets with similar astrophysical characteristics to Earth. Earth-like exoplanets are the most promising candidates that will assist our understanding of how Earth evolved in our solar system, thus determining the unique evolution of life. To date, there have been 5,090 confirmed exoplanets (as of 19 September 2022) discovered orbiting nearby stars (Williams 2017; Caltech 2021). Due to the observational and technological limitations, the number of these confirmed exoplanets that are known to be Earth-like remains inconclusive (Caltech 2021). Because Earth-like exoplanets are of particular interest, our understanding of other types of terrestrial exoplanets is also limited, resulting in an adverse effect on the progress of terrestrial exoplanet research.

To account for these limitations, current methods must be refined to improve our understanding of all terrestrial exoplanets which may enhance the search for Earth-like exoplanets and planetary systems similar to our solar system, both now and in the future. The research in this project will look to Venus-like exoplanets as an alternative target to Earth-like exoplanets. Venus-like exoplanets are suggested here

due since they are likely to display unique spectral features that are will be easily detectable by current and emerging instrumentation of space-based observatories. This method could assist the identification of planetary systems with the stability to contain other terrestrial exoplanets. Expanding the research to other types of terrestrial exoplanets may also assist the refinement of the current classification of terrestrial exoplanets.

This thesis will give a literature review (Chapter 2) of the current knowledge of our Solar System, including an overview of the Sun, Earth, and Venus. The detection methods used for exoplanetary discoveries as well as the databases to be used in the methodology will also be detailed. Chapter 3 states the aims and research question that will be explored in this project. Chapter 4 will discuss the methodology used in this project, along with the installation of the simulation programs and any troubleshooting regarding the methods. The results to date will be found in Chapter 5 which will be discussed and analysed in Chapter 6. Finally, concluding remarks on the project will be made in Chapter 7.

CHAPTER 2: LITERATURE REVIEW

2.1 Planetary Systems including our Solar System

Our Solar System contains a total of eight main planets, four of which are terrestrial or rocky planets (i.e. Mercury, Venus, Earth and Mars) where Earth is the only planet known to be inhabited by modern forms of life. The four remaining planets that reside in our Solar System are Jovian or gas giant planets (i.e. Jupiter, Saturn, Uranus and Neptune) (NASA 2021). Note that this project is not concerned with Jovian planets however, they will be discussed in later section to emphasise the current limitations of exoplanet research. The understanding of our solar system is quintessential for identifying similarities displayed in other planetary systems and thus, the possibility of finding terrestrial exoplanets.

2.1.1 Solar-Type Stars and the Sun

Our Sun is ~4.5 billion years old with a mass and radius of 1.989×10^{30} kg and 6.955×10^{8} m, respectively (Barnett 2018). Its luminosity is 3.84×10^{26} Watts (CSIRO 2021). Because of its mass, luminosity, and evolutionary status, the Sun is classified as a G2V (or G2 dwarf) star according to the Harvard Classification Scheme, where "G" is the spectral type, "2" is the spectral sub-class, and "V" is the luminosity class. For the case of the Sun, the "V" indicates that it is a dwarf star(Swinburne University of Technology 1999). Stars that have similar characteristics to our Sun are referred to as solar-type stars or solar analogs (Wilson 1978). Since it is difficult to determine the exact properties of stars, the search for solar analogs is broadened by using a range of spectral types (Soderblom & King 1997). In accordance with the Harvard

Classification Scheme, solar analogs have spectral types that range between K2V through to F8V (Soderblom & King 1997). However, exoplanets have also been found around M-dwarfs such as the TRAPPIST-1 system (Gillon et al. 2016). It is important to determine the star's spectral type to narrow the number of planetary systems that may contain exoplanets similar to those found in our solar system.

2.1.2 Our Home Planet – Earth

Since life is only known to exist on Earth, the geophysical features (i.e. surface liquid water, active tectonic plates, a magnetic dynamo and an atmosphere abundant in greenhouse gases (specifically nitrogen gases (N_2)) exhibited on Earth can be used to guide the search for life on other planets. Modern Earth's atmosphere is abundant in gases such as methane (CH_4), nitrous oxide (N_2O), chloromethane (CH_3Cl) and carbonyl sulfide (COS), as a result of the feedback from life (Kasting & Siefert 2002). This has greatly impacted the long-term stability of Earth's climate (Charnay et al. 2020).

2.1.3 Venus: Earth's Evil Twin

Venus, also known as "Earth's evil twin", is similar to Earth in both size and bulk atmospheric composition (Hall 2019). However, the environments that occupy these worlds vary significantly from each other. That is, Earth is wet, temperate and suitable for modern life, and Venus is hot and uninhabitable (Kane et al. 2019). Theories suggest that Venus once accommodated a similar environment to Earth and

was formerly suitable for life of some kind (Kane et al. 2019). The factors that diverged the evolutionary paths of Earth and Venus remain inconclusive.

As seen in Table 1, Venus' current atmospheric composition predominantly consists of carbon dioxide (CO_2) with small traces of nitrogen (N_2), argon (Ar), sulphur dioxide (SO_2), carbon monoxide (CO) and helium (He) (Lammer et al. 2018). Venus' atmosphere is less abundant in atmospheric water vapours (H_2O), where Venus has approximately 2.3×10^5 times less atmospheric H_2O than Earth (Kane et al. 2019). In contrast to Earth, the pressure of the Venus atmosphere is 92 times that of Earth (i.e. 92 bar atmosphere). It also has a surface temperature of approximately 735 Kelvin (K) (Taylor et al. 2018) whereas Earth's surface temperature is 288 K (Williams 2019). Although Venus' extreme temperature is partially due to its close orbital distance from the Sun (~0.72 au), this is a direct result of outgassing from volcanic activity on Venus (Way et al. 2016). The volcanoes present on Venus have emitted large amounts of CO_2 and SO_2 into its atmosphere (Taylor et al. 2018) and has also contributed to the abundance of sulphuric acid (H_2SO_4) in Venus' upper atmosphere (Luginin et al. 2016). Prior to the outgassing from volcanic activity, Venus' ancient atmosphere may have had similar characteristics to the atmosphere of modern Earth. Global climate models developed by Way et al. (2016) showed that the ancient Venus atmosphere, assuming that there was 100% cloud coverage, was likely to be abundant in N_2 with small traces of CO_2 and CH_4. Because Way et al. (2016) only modelled ancient Venus' atmosphere with clouds, it is uncertain how a cloud-free model would affect the detection of other gases present in ancient Venus' atmosphere.

Table 1: Percentage of atmospheric species present in the Venus and Earth atmosphere. Modified from Lammer et al. (2018, p. 2) unless stated elsewhere.

Species	Venus	Earth
CO_2	96.5%	0.0407%
N_2	3.5%	78.084%
H_2O	0.002%[1]	~0.25%[2]
O_2	-	20.946%
Ar	0.007%	0.9340%
SO_2	0.015%	-
CO	0.0017%	0.00001%[3]
He	0.0012%	0.00052%[3]

[1] NASA 2021, Available at: https://nssdc.gsfc.nasa.gov/planetary/factsheet/venusfact.html

[2] Trenberth & Smith 2005, Available at: https://journals.ametsoc.org/view/journals/clim/18/6/jcli-3299.1.xml

[3]Shapley 2010, Available at: http://butane.chem.uiuc.edu/pshapley/environmental/l12/2.html

2.1.3.1 Structure of modern Venus' atmosphere

The *Pioneer* probe that ventured through Venus' atmosphere in 1978 showed extensive and varying layers of clouds and haze (Taylor et al. 2018). The layers of clouds and haze can be subdivided into three main sections; the Upper Haze, the Upper Cloud and the Middle and Lower Clouds (Titov et al. 2018).

The Upper Haze and Upper Cloud have an optical thickness of approximately 40 km and contains high concentrations of H_2SO_4 (Luginin et al. 2016). Exploratory missions into Venus have also detected large amounts of non-sulphuric acid aerosols such as chlorine (Cl), phosphorus (P), and iron compounds within this region of the atmosphere (Markiewicz et al. 2007). Because the Upper Cloud layer is so thick, it obscures the visibility of anything that resides below it, making it the only layer visible from space (Basilevsky & Head 2003). The Middle and Lower Clouds also contain

H_2SO_4 however, due to the change in atmospheric temperature and pressure, H_2SO_4 becomes thermodynamically unstable and begins to evaporate due to the conditions at this altitude (Titov et al. 2018; Ando et al. 2020).

During the missions to Venus, the time available for data collection was limited since the probes malfunctioned upon reaching Venus' surface (Voytek 2009). Because of this, there is currently an insignificant amount of information on the structure of Venus' atmosphere and it will require further attention in future missions (Voytek 2009).

2.1.4 The Temperate Zone

The term "Habitable Zone" was rendered in the 19th Century which defined the distance between a planet and its host star where liquid water could exist, and life could evolve (Ligman 2021). However, this term is specific to the structure of our solar system and the detection of habitability within it (Ligman 2021). Many astronomers now use the term Temperate Zone (Niraula et al.) since it defines the zone around the host star where stable liquid medium may exist on a planet (Hill 2018). This term also shifts the focus onto the effects of stellar radiation on a terrestrial planet rather than the detection of life (Tasker et al. 2017).

Both Venus and Earth are located relatively close to the Sun at 0.72 au and 1 au, respectively (California Institute of Technology 2019). The range of the TZ is approximated to be between 0.99 au (the inner edge) to 1.70 au (the outer edge) from the Sun (Wilson et al. 2021). The inner edge of the TZ is the minimum distance from the star for a planet to be able to retain liquid water on its surface (Way et al.

2016). The outer edge of the TZ identifies a planet's ability to retain a CO_2-rich atmospheres (Kopparapu et al. 2013). Note that the quantity of CO_2 in a planet's atmosphere determines whether the planet will experience a greenhouse effect. With this effect, the planet's surface temperature increases which allows liquid medium to reside on its surface (Wordsworth & Pierrehumbert 2012).

The evolution of a star causes the boundaries of the TZ to change over time and therefore, altering the planet's geophysical characteristics such as its atmospheric properties and surface temperature (Wilson et al. 2021). However, a planetary system that has a stable TZ (i.e. the range of the TZ does not vary greatly over time) is more likely to contain potential habitable worlds (Agnew et al. 2019). Unstable TZs can be caused by the rapid increase in a star's luminosity in a relatively short period, preventing the evolution of life within this time (Planetary Sciences Inc. 2019). Also, if a gas giant planet is present in the TZ, it is assumed that any terrestrial planets within the gas giant's vicinity could not exist. This is because the terrestrial planet would be consumed by the strong gravitational pull of the gas giant (Planetary Sciences Inc. 2019). Although the TZ is important for determining the location of Earth-like exoplanets, it is not suitable for locating Venus-like exoplanets. The region that a Venus-like exoplanet may be detected is referred to as the Venus Zone.

2.1.4.1 The Venus Zone

The Venus Zone (VZ) is the distance that the terrestrial planet is situated from its host star that allows the planet to have a Venus-like atmosphere. That is, a terrestrial planet that is experiencing a runaway greenhouse effect in its atmosphere, or its atmosphere is losing mass due to its proximity to its host star (Kane et al. 2019). Like the TZ, the VZ also has an inner and outer edge as shown in Figure 1. The boundaries for these zones are determined by the percentage of stellar radiation emitted onto the planet relative to the stellar radiation emitted onto Earth from our Sun.

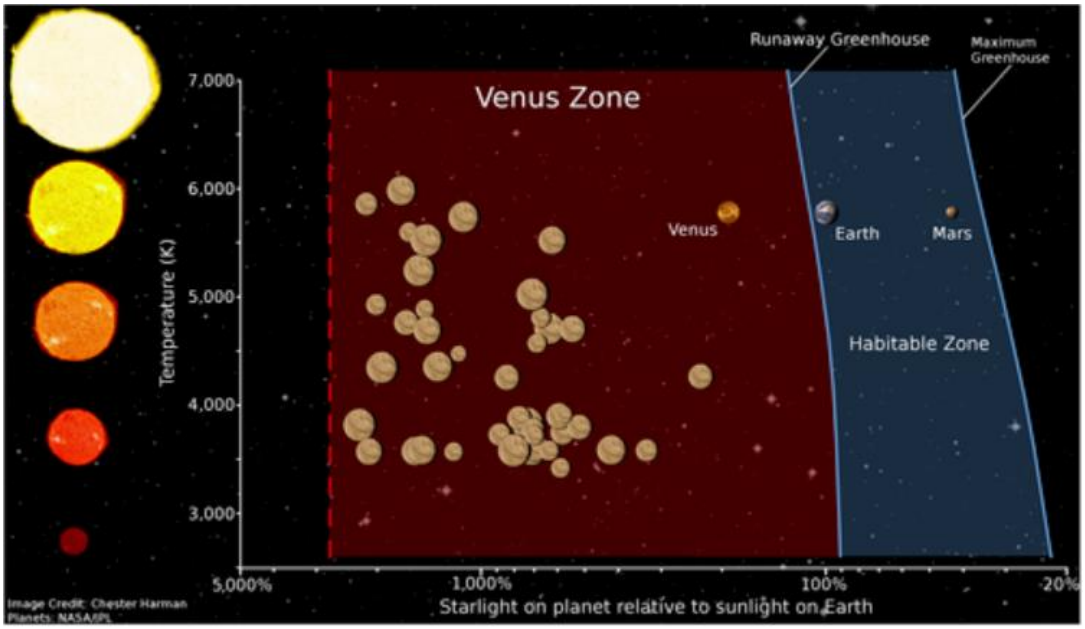

Figure 1: Diagram of the relative distances of the inner and outer boundaries of the Venus Zone (VZ) and the Temperate Zone (Niraula et al.) for stars at different temperatures. Note that this diagram refers to the TZ as the Habitable Zone. The y-axis represents the temperatures of the star in Kelvin (K) and the x-axis represents the percentage of stellar radiation emitted onto the planet using a logarithmic scale. This percentage is relative to the percentage of stellar radiation emitted onto Earth from our Sun. The diagram also depicts the locations of Venus, Earth, and Mars in relation to our Sun, as well as current terrestrial candidates that have been observed in the VZ. Note that the size of each planet is relatively represented in this diagram. Sourced from Kane et al. (2019, p. 2022).

The outer edge of the VZ, which is also the inner edge of the TZ, is the distance from the host star where a planet will experience ~3000% of stellar radiation relative to the percentage of stellar radiation emitted onto Earth from our Sun (see Figure 1) (Kane et al. 2019). At this distance from its host star, the planet may experience a runaway greenhouse effect if there are moderate levels of CO_2 present in the atmosphere (Kane et al. 2014). On the other hand, the inner edge of the VZ is the distance from the host star where a planet will experience ~90% of stellar radiation relative to the percentage of stellar radiation emitted onto Earth from our Sun (see Figure 1) (Kane et al. 2019). At this distance from the host star, the planet may experience atmospheric erosion. In other words, there would be significant loss of the planet's atmospheric mass (Kane et al. 2014). According to Figure 1, the region of the VZ is greater than that of the TZ, suggesting that there is also a greater chance of finding a Venus-like candidate than an Earth-like exoplanet.

2.2 Detection Methods

Currently, terrestrial exoplanets are difficult to observe with current detection methods due to their relative size and orbital distance from their host star (Udry & Santos 2007). In saying this, the challenge of detecting terrestrial exoplanets does not imply that they cannot be found, but rather the quantity of terrestrial exoplanets detected is significantly less compared to the detection of larger exoplanets like gas giants. The two most successful methods for detecting exoplanets orbiting nearby stars are radial velocity and the transit method. Both methods have, and still are, detecting and confirming large quantities of all types of exoplanets.

2.2.1 Radial Velocity

Radial velocity is the primary detection method for discovering exoplanets to date. Via spectroscopy, this method is able to detect the radial reflex motion when a planet interacts with its host star (Wright & Gaudi 2013). In other words, it can detect the small movements of the star's position due to the gravitational pull of the planet (or multiple planets) orbiting the star (Yaqoob 2011). As seen in Figure 2, the star orbits in a small circle or ellipse around the system's centre of mass due to the gravitational pull of a planet. This change in position makes the star appear to "wobble" which allows the observer to determine if a planet is orbiting the star or not.

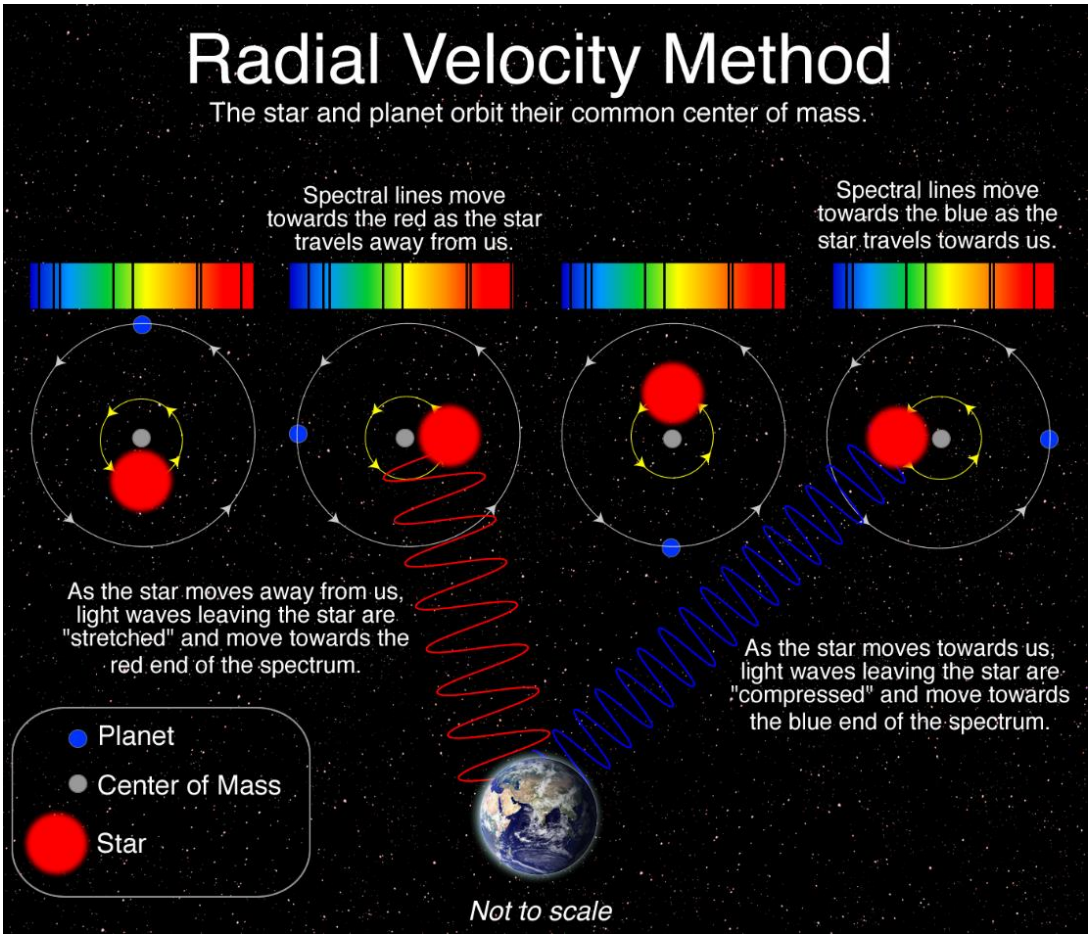

Figure 2: Diagram of the radial velocity method. This method is used to detect exoplanets by looking for small changes in star's position caused by the gravitational pull of an orbiting planet. When the star moves away from the observer (and the planet moves towards the observer), the spectral lines are red shifted. When the star moves towards the observer (and the planet moves away from the observer), the spectral lines are blue shifted. Sourced from Williams (2017).

This "wobble" or radial reflex motion is confirmed through spectroscopy by measuring the Doppler shift of the star's spectrum. When the star moves away from the observer, the wavelengths detected appear elongated or red shifted, and when the star moves towards the observer, the wavelengths detected appear compressed or blue shifted (Wright 2018).

This radial reflex motion of the star-planet interaction can determine the orbital period, distance from the star, eccentricity, and mass of a planet (Wright & Gaudi 2013). Since larger planets cause a larger reflex motion of the host star, this detection method is biased against small, terrestrial exoplanets. In saying this, the minimum detectable size and mass of an exoplanet becomes smaller as the orbital distance decreases. This means that it is easier to detect planets with shorter orbital distances regardless of its size and mass (NASA 2017).

2.2.2 The Transit Method

The transit method is arguably the simplest method for detecting exoplanets (Wright & Gaudi 2013) and accounts for approximately 70% of all exoplanet detections (Deeg & Alonso 2018). As the name suggests, an exoplanet is detected with this method when it transits. That is, it passes directly in front or behind the star with respect to the observer's perspective (see Figure 3). When the exoplanet passes in front of the star, it is referred to as a primary transit. When it passes behind the star, it is then referred to as a secondary transit (Encrenaz 2014).

When a primary transit occurs, the brightness of the star is reduced for a period of time (Wright & Gaudi 2013). Depending on the amount of light from the host star that is blocked by the exoplanet, its radius can also be resolved as a percentage of the stellar radius. This radius can then be used to determine other characteristics of the exoplanet such as the atmospheric composition and temperature. This is because the radius of the exoplanet is inferred by the specific wavelengths of molecular species present in the exoplanet's atmosphere (Encrenaz 2014). Note that this

method is only applicable when the exoplanet passes in front of the star with respect to the observer's perspective to ensure that the dimming of the star's brightness can be observed (Santos & Amorium 2017).

Primary transits are more commonly used than secondary transits for exoplanet detection, particularly terrestrial exoplanets. This is because the size of a terrestrial exoplanet is relatively small compared to a larger gas giant exoplanet, which means that the effects that are detectable during a secondary transit are less likely to occur for smaller terrestrial exoplanets (Santos & Amorium 2017).

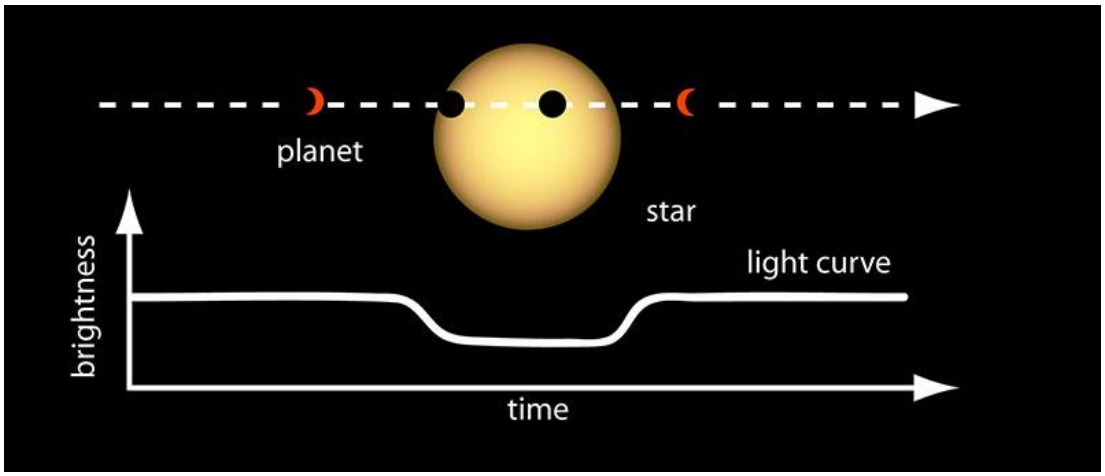

Figure 3: Diagram of the transit method. This method measures the change in the brightness of the star as a planet passes in front of it with respect to the observer's perspective. In the diagram, the change in brightness is indicated by the light curve where the light curve dips as the planet transits in front of the star. Sourced from NASA Ames (2021).

2.2.3 Simultaneous Spectroscopy and the Transit Method

The transit method can also be used in conjunction with spectroscopy to analyse the transmission absorption spectrum and emission spectrum of the exoplanet and its host star. As mentioned in section 2.2.2, a primary transit occurs when the exoplanet transits in front of the star with respect to the observer's perspective. When this occurs, a unique spectral "fingerprint" of the combined star and planet's spectrum is created (Rugheimer et al. 2013). When the exoplanet completes a secondary transit, that is, it passes behind the star, only the star's emission spectrum can be observed independently of the exoplanet (Hoeijmakers et al. 2018). By comparing the two spectral "fingerprints" of the primary and secondary transits, the exoplanet's emission spectrum can be identified (Barstow et al. 2015).

The exoplanet's transmission absorption spectrum is determined during a primary transit. When the light from the star passes through the exoplanet's atmosphere during a primary transit, the molecular species that are present in the atmosphere absorb specific wavelengths, thus allowing for the chemical composition of the exoplanet's atmosphere to be observed. The absorption of light is also affected by other factors in the atmosphere such as Rayleigh Scattering. Rayleigh Scattering causes light passing through an atmosphere to "scatter" or refract due to the light's interaction with the small gas molecules present in the atmosphere (Hansen & Travis 1974). Examples of molecules that cause Rayleigh Scattering are O_2, He and N_2 (Climate Policy Watcher 2022). The effects of Rayleigh Scattering can alter the transmission absorption spectrum by reducing the absorption of molecules at shorter wavelengths such as ultraviolet (Niraula et al.) and visible, thus changing the

overall planet spectra (Robinson et al. 2017). By interpreting the transmission absorption spectrum and considering the effects of Rayleigh Scattering within terrestrial exoplanet atmospheres, molecular constituents can be identified within their atmospheres (Chance & Spurr 1997).

2.2.3.1 Detection and Characterisation of Venus-like Exoplanets

Most terrestrial exoplanets have been discovered in the VZ when using the transit method since there is an observational bias towards exoplanets with shorter orbital periods (Kane et al. 2019).

Because the exoplanet is located at close proximity to its host star, the amount of stellar radiation emitted onto it would cause the exoplanet to display unique atmospheric spectral features that are optimal for characterisation. Exoplanets that have shorter orbital periods are most likely to display runaway greenhouse spectral features like that of Venus (Kane et al. 2018). This means that Venus-like exoplanets are likely to be discovered in the VZ because of the spectral features that they are expected to display. Kane et al. (2014) showed that this is quantifiable, where it was determined that terrestrial exoplanets likely to display runaway greenhouse spectral features have an occurrence rate of ~0.32 and ~0.45 when sampled from 22 M dwarfs and 21 G-K dwarfs, respectively.

Not only are the detection methods important for the discovery of Venus-like exoplanets, but the capabilities of the instrumentation used to detect them also have a significant impact on the outcome of exoplanet observations.

2.3 Space Telescope Instrumentation

Telescopes are important astronomical instruments used to observe objects beyond Earth and within our universe. They can be either ground- or space-based. Space telescopes are superior to ground-based telescopes in terms of exoplanet research. This is because space telescopes are able to detect a wider range of frequencies and wavelengths of the electromagnetic spectrum that may be undetectable due to the interference of Earth's atmosphere (University of Arizona 2016). The interference of Earth's atmosphere can cause issues when looking for specific molecules expected to be found in Earth- and Venus-like atmospheres (University of Arizona 2016). Space telescopes have been able to detect and confirm thousands of exoplanets orbiting nearby star systems, including small, inner, terrestrial exoplanets. Table 2 lists the space telescopes that have been launched and have contributed to exoplanet discoveries to date.

Table 2: The fleet of space telescopes that have contributed to exoplanet discoveries.

Telescope	Lifespan	Wavelength	Contributions
Hipparcos[1]	1989 – 1993	Optical	• Observed and catalogued the precise position of 118 2018 stars
Hubble Space Telescope (HST)[2]	1990 – present	UV, Optical & Near IR (0.115 – 1.7 μm)	• Observed the first confirmed discovery of a transiting exoplanet • Detected the first organic molecule in exoplanet atmospheres
Spitzer[3]	2003 – 2020	Infrared (3.6 – 16 μm)	• First telescope to detect light directly from distant exoplanet • Determined the geophysical parameters of distant planets through its IR capabilities • Detected exoplanets through the transit method
Convection, Rotation and planetary Transit telescope (CoRoT)[4]	2006 – 2013	Optical	• Designed specifically to search for terrestrial exoplanets using the transit method • Able to calculate a star's mass, age and chemical composition via 'starquakes'
Kepler/K2[5]	2009 -2018	Optical (0.43 – 0.89 μm)	• Designed to determine the characteristics of exoplanets and their planetary systems • Used the transit method to detect exoplanets
Gaia[6]	2013 – present	Optical, Near IR (0.33 – 1.05 μm)	• Precisely measure and catalogue stars, including information on their position, distance, movement, and magnitude
Transiting Exoplanet Survey Satellite (TESS)[7]	2018 – present	Optical, Near IR (0.6 – 1 μm)	• Searching for exoplanets using the transit method

Telescope	Lifespan	Wavelength	Contributions
			• Cameras are capable of detecting terrestrial exoplanets • Set to monitor over 200 000 stars for transiting exoplanets
Characterising ExOPlanets Satellite (CHEOPS)[8]	2019 – present	Optical, Near IR (0.4 – 1.1 µm)	• Characterise exoplanets orbiting bright, nearby stars • Has made precise observations of transiting exoplanets, particularly super-Earths and Neptune-like exoplanets
James Webb Space Telescope (JWST)[9]	2021 – present	Optical, IR (0.6 – 28.8 µm)	• Will observe the formation and evolution of confirmed exoplanets and their planetary systems

[1] ESA 2022, Available at: https://www.cosmos.esa.int/web/hipparcos

[2] Space Telescope Science Institute 2022, Available at: https://hubblesite.org/mission-and-telescope, https://hubblesite.org/science/exoplanets

[3] Caltech n.d., Available at: https://www.spitzer.caltech.edu/mission/exoplanets

[4] Caltech n.d., Available at: https://www.esa.int/Science_Exploration/Space_Science/COROT_overview

[5] Johnson 2018, Available at: https://www.nasa.gov/mission_pages/kepler/overview/index.html

[6] ESA n.d., Available at: https://www.esa.int/Science_Exploration/Space_Science/Gaia_overview

[7] Garner 2020, MIT n.d., Available at: https://www.nasa.gov/content/about-tess, https://tess.mit.edu/science/

[8] ESA n.d., Available at: https://www.esa.int/Science_Exploration/Space_Science/Cheops, https://sci.esa.int/web/cheops

[9] NASA 2022, Available at: https://jwst.nasa.gov/

There are many space telescopes famous for their success in finding exoplanets, particularly the Hubble Space Telescope, Spitzer, Kepler/K2, and the Transiting Exoplanet Survey Satellite. These telescopes will be discussed in more detail in the following sections.

2.3.1 The Hubble Space Telescope

In 1990, NASA launched its first major optical space telescope, known as the Hubble Space Telescope (HST), as part of their Great Observatories Program. For over 30 years, HST has been orbiting 547 km above Earth's surface, making millions of observations, and expanding our current knowledge of the universe (Belleville 2021). HST contains an abundance of science instruments that are capable of observing a wide variety of astronomical objects at a range of different wavelengths.

2.3.1.1 HST Instruments and Specifications

The science instruments on the HST include the Space Telescope Imaging Spectrograph (STIS), the Cosmic Origins Spectrograph (COS), the Advanced Camera for Surveys (ACS) and Wide Field Camera 3 (WFC3) (Space Telescope Science Institute 2022a). Below in Table 3 and 4 are the specifications of the instruments currently in operation on the HST. In this section, only the HST instruments that have contributed to exoplanet discoveries will be discussed.

The STIS is an instrument used for spectroscopy. This instrument consists of one charged-coupled device (CCD) and two multi-anode microchannel arrays (MAMA).

The CCD is used to detect near infrared (NIR) light whereas the two MAMA are used to detect ultraviolet light (Garner 2019; ICNIRP 2020). The wavelength range of all the devices in the STIS are between 0.115 to 1 micrometre (μm). Because of its wavelength range, the STIS is capable of capturing highly resolved spectra of objects in the optical, NIR and UV spectrum (Garner 2019). The STIS is often used in conjunction to the COS instrument since both devices are used for spectroscopy and have capabilities which complement each other (Garner 2019).

The ACS instrument was originally designed to survey extensive areas of the sky but is capable of observing faint objects within the universe (Garner 2017b). The detectable wavelengths of the devices in the ACS instrument range between 0.115 to 1.05 μm, meaning that it can detect wavelengths from UV to NIR (Garner, 2017). The ACS is mainly used to study weather patterns on other planets within our solar system (ESA 2022c).

The COS instrument is another spectrograph on board the HST. The COS has two channels: the near ultraviolet (NUV) and far ultraviolet (FUV) channel. The NUV observes near UV wavelengths (0.170 to 0.320 μm), and the FUV observes far UV wavelengths (0.115 to 0.205 μm) (ESA 2022a). It is used to observe the formation and evolution of objects such as exoplanets (ESA 2022a).

Like the ACS, the WFC3 instrument is used to observe the formation and evolution of stars and planets (ESA 2022b). Because its camera has a wider field of view with a higher resolution, it is able to observe a wider range of wavelengths than the ACS instrument. The wavelengths that the WFC3 can detect is within the UV and NIR spectrum (0.200 to 1.70 μm).

Table 3: Specifications of HST's STIS and ACS instruments.

Instrument	Instrument Type	Field of View (arcseconds)	Wavelength range (µm)
STIS[1]	Camera + Spectrograph	MAMA – 25 × 25 CCD – 50 × 50	0.115 – 1.00
ACS[2]	Camera	WFC – 202 × 202 HRC – 29.1 × 26.1 SBC – 1024 × 1024	WFC – 0.35-0.15 HRC – 0.200-1.05 SBC – 0.115-0.18

[1] ESA 2022, Available at: https://esahubble.org/about/general/instruments/stis/

[2] ESA 2022, Available at: https://esahubble.org/about/general/instruments/acs/

Table 4: Specifications of HST's COS and WFC3 instruments.

Instrument	Instrument Type	Channel	Detector Type	Field of View (arcseconds)	Wavelength Range (µm)
COS[1]	Spectrograph	FUV	X-delay line	-	0.115-0.205
		NUV	NUV MAMA	-	0.170-0.320
WFC3[2]	Camera	UVIS	Si	160 × 160	0.200-1.000
		NIR	HgCdTe	123 × 137	0.850-1.700

[1] ESA 2022, Available at: https://esahubble.org/about/general/instruments/cos/

[2] ESA 2022, Available at: https://esahubble.org/about/general/instruments/wfc3/

The WFC3 instrument's capabilities were used to dictate the ideas for the instruments on board the recently launched James Webb Space Telescope (Garner 2017a).

2.3.1.2 Capabilities and Limitations of HST

Currently, the HST is the only space telescope that is able to provide high resolution images in UV, optical and NIR wavelengths (NASA 2020). Because of this, the HST is capable of observing exoplanet atmospheres by differentiating the spectra of the star

and the exoplanet's atmosphere via Rayleigh Scattering (Sing et al. 2013). However, the atmospheres of small, inner terrestrial exoplanets like Earth and Venus become more difficult to characterise since the range of wavelengths are limited by the capabilities of the HST's instruments. This also limits the types of molecules that can be detected in such atmospheres and thus limits the ability to find Venus- and Earth-like exoplanets. As mentioned in Table 3 and 4, the range of wavelengths that can be observed by the HST instruments ranges from UV to NIR wavelengths (~0.115 to 1.700 μm). The molecules and their associated isotopes that have the strongest signals and can be detected in this wavelength range include H_2O ($H_2{}^{16}O$), and O_2 ($^{16}O_2$).

The HST's ability to detect molecular species within the atmospheres of small gaseous (possibly terrestrial) exoplanets orbiting TRAPPIST-1 was demonstrated by de Wit et al. (2018). de Wit et al. (2018) specifically analysed the transmission absorption spectrum of TRAPPIST-1d, TRAPPIST-1f, TRAPPIST-1e and TRAPPIST-1g. The Mikulski Archive for Space Telescopes database was used to obtain light curve observations of each TRAPPIST-1 exoplanet. These observations were collected by the HST WFC3 instrument. The light curves of the exoplanets were then analysed using the Markov chain Monte Carlo software and a custom Fortran 90 code (see de Wit (2018)). By developing the transmission absorption spectral models of the TRAPPIST-1 system, de Wit et al. (2018) was able to analyse the abundance of molecules for each exoplanet. The molecules used to model the spectra were CO_2, CH_4, N_2, H_2O and H_2 with a 3σ uncertainty for all exoplanets. As shown in Figure 4, H_2 molecules did not converge to the observation of any of the TRAPPIST-1 exoplanets. The article suggests the likelihood of the TRAPPIST-1 exoplanets being terrestrial

exoplanets since the models for H_2O, N_2 and CO_2 slightly converge to the observations. However, the detection of strong molecular signals of H_2O, N_2 and CO_2 cannot be achieved with HST WFC3 due to the relatively low resolution and small wavelength range between 0.85 and 1.7 µm (see Table 4) which is suggested by the relatively small transit depths of each exoplanet observation as seen in Figure 4. HST's inability to detect strong molecular signals means that other instrumentation should be favoured for analysing terrestrial exoplanet atmospheres.

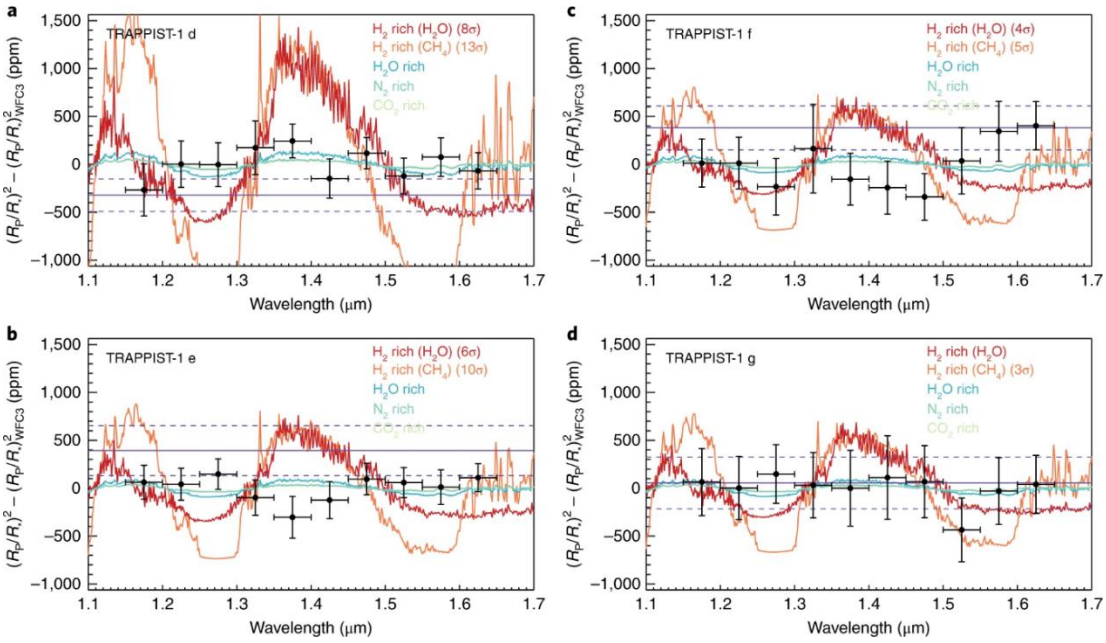

Figure 4: Models of the transmission absorption spectrums of four of the TRAPPIST-1 exoplanetary system using a 3σ uncertainty. Exoplanets in the figure include TRAPPIST-1d, TRAPPIST-1f, TRAPPIST-1e and TRAPPIST-1g. The x-axis represents the wavelength in microns (µm) as a logarithmic scale, and the y-axis represents the calculated transit depth in parts per million (ppm). The observations were developed from four observation points collected by the Hubble Space Telescope's Wide Field Camera 3 (HST WFC3) instrument. The spectra were then analysed using the Markov chain Monte Carlo software and a custom Fortran 90 code. Sourced from de Wit et al. (2018).

The detection of molecules like H_2O in terrestrial exoplanet atmospheres by the HST instruments was reported by Kreidberg et al. (2014). They determined that the spectral features of heavier molecules like H_2O may be detectable in terrestrial exoplanet atmospheres since such molecules present absorption features that can be identified in the NIR spectrum (Kreidberg et al. 2014). Molecules that are not within this wavelength range or do not have a strong enough signal and cannot be detected by the HST. This includes molecules such as CH_4 ($^{12}CH_4$), CO_2 ($^{12}C^{16}O_2$) and N_2 ($^{14}N_2$) (Quanz et al. 2021; Gordon et al. 2022). Note that the isotopes listed with these molecules are the most abundant within this wavelength range. Further information about these isotopes can be found in the HITRAN database (Gordon et al. 2022). The molecules that cannot be detected by the HST instruments are the same molecules expected to be found in the atmospheres of Venus- and Earth-like exoplanets. This suggests that the HST may not be capable of categorising such exoplanets despite being able to find them. Some objects are also too distant and or too cold to emit wavelengths in the optical to NIR wavelengths, therefore these objects cannot be detected by the HST instruments (Quanz et al. 2021). Because of HST's observational limitations, any future space-based telescopes will consider these limitations for improved detections of the atmospheres of exoplanets where improvements on the levels of HST discussed here would be ideal. NASA's other telescopes such as the Spitzer Space Telescope, the Kepler telescope, and the Transiting Exoplanet Survey Satellite (TESS), compliment the discoveries of HST and further its research.

2.3.2 The Successors of the Hubble Space Telescope

2.3.2.1 The Spitzer Space Telescope

Launched in 2003 as part of NASA's Great Observatory Program, the Spitzer Space Telescope was one of the first space telescopes specific to infrared (IR) astronomy. Its initial mission was to study a variety of objects from within our Solar System and the distant universe (McGregor et al. 2022). However, in 2009, issues with the telescope caused a re-evaluation of the Spitzer missions and it began studying specifically the expansion of the universe and asteroid characterisation. Spitzer also went on to study the atmospheres of exoplanets, in particular gas giants (McGregor et al. 2022). The instruments on board Spitzer were able to observe wavelengths in IR, from near to far IR (2.4 to 38 μm) (Caltech 2022). Because of its instrument's capabilities, Spitzer used the transit method to detect exoplanets, becoming the first space telescope to detect light directly from exoplanets within a planetary system (NASA 2022b). It also determine geophysical characteristics of larger exoplanets through spectral analysis, including the identification of their atmospheric compositions (NASA 2022b). After 16 years, Spitzers missions finally ended in 2020 however, its legacy lives on in space telescopes specific to exoplanet detections, such as Kepler and TESS (NASA 2022b).

2.3.2.2 The Kepler/K2 Missions

In 2009, NASA's Kepler space telescope was launched where its primary objective was to find Earth-sized exoplanets using the transit method. However, in 2011, Kepler faced mechanical issues which caused parts of the telescope's instrument to

become unusable (Pyle 2020). NASA then designed the K2 mission, which would continue the use of the Kepler space telescope to detect a variety of different exoplanets instead of specifically targeting Earth-sized exoplanets (Mighell & van Cleve 2020).

The Kepler/K2 telescope carries one instrument: a photometer (Pyle 2020). Composed of 42 CCDs, this photometer observes wavelengths between 0.4 and 0.85 µm. This instrument has the ability to measure the light from distant stars and observe transiting exoplanets within that star's system (Johnson 2017). After identifying over 2000 transiting exoplanets, the Kepler/K2 mission came to an end in 2018 (Pyle 2020).

2.3.2.3 The Transiting Exoplanet Survey Satellite

In 2018, NASA launched the successor of Kepler/K2, the Transiting Exoplanet Survey Satellite (TESS) (Garner 2020). TESS contains four identical wide-field CCD cameras which are able to observe wavelengths from 0.6 to 1.04 µm (Vanderspek et al. 2018). The four cameras allow TESS to collect high-resolution images of its targets (MIT 2022). Like the Kepler/K2 mission, TESS also detects exoplanets using the transit method. However, TESS can specifically target exoplanets that orbit within the TZ (Pyle 2021). Like all photometry-based space telescopes, TESS requires the use of other telescopes to confirm exoplanets as well as measure the spectrums of the stars and exoplanets since it does not have the instruments to do so itself (MIT 2022). In 2020, the primary mission of TESS concluded, confirming the existence of 66 new exoplanets and nearly 2100 exoplanet candidates to be confirmed. To this day, TESS

continues to search for small, terrestrial exoplanets in its extended mission (Brennen 2021).

Although both the Kepler/K2 and the TESS missions contributed greatly to the search for exoplanets, they were not designed with the same capabilities as the HST instruments such as having the ability to perform spectroscopy. Both telescopes were also limited to using the transit method to find exoplanets. This meant that a lot of the exoplanets that Kepler/K2 and TESS found, had to be confirmed by external sources such as ground-based telescopes. Because of their limitations, NASA designed a larger, more equipped telescope, known as the James Webb Space Telescope, that would follow in the footsteps of the HST.

2.3.3 The Future Endeavors of the James Webb Space Telescope

Launched on the 25th of December 2021, the James Webb Space Telescope (JWST) is expected to expand upon the discoveries made by HST, Kepler/K2 and TESS. JWST will be able to precisely observe the evolution of the universe as well as characterize the atmospheres of exoplanets (Barstow et al. 2015). Like the HST, the JWST contains a number of instruments capable of completing planned research goals of previous space telescopes, including the observation of the early universe and continuing the research on exoplanets (Barnett 2022).

2.3.3.1 JWST Instruments and Specifications

Similar to the HST, the JWST has four instruments: the Mid-Infrared Instrument (MIRI), the Near-Infrared Camera (NIRCam), the Near-Infrared Imager and Slitless

Spectrograph (NIRISS), and the Near-Infrared Spectrograph (NIRSpec) (Space Telescope Science Institute 2020). Below in Table 5 are the specifications of the instruments on the JWST. In this section, only the instruments on the JWST that will contribute to exoplanet research will be discussed.

MIRI operates as a combined imager and spectrograph that covers the mid-IR wavelengths (4.9 to 28.8 µm) (Space Telescope Science Institute 2020). The imager has a wavelength range from 5.6 to 25.5 µm whereas the spectrographs wavelength range is from 0.5 to 1.2 µm (Space Telescope Science Institute 2022b). The spectrograph uses both slitted and slit-less spectroscopy (Space Telescope Science Institute 2020). The main purpose of MIRI will be to image exoplanets and measure the spectra of transiting exoplanets (Reike et al. 2015).

Table 5: Specifications of JWST's MIRI, NIRCam, NIRISS and NIRSpec instruments.

Instrument	Instrument Type	Field of View (arcseconds)	Wavelength range (µm)
MIRI[1]	Imager + Spectrograph	74 × 113	4.9 – 28.8
NIRCam[2]	Imager + Coronagraph + Spectrograph	132 × 132	0.6 – 5.0
NIRISS[3]	Imager + Slitless Spectrograph	132 × 132	0.6 – 5.0
NIRSpec[4]	Spectrograph	204 × 216	0.6 – 5.3

[1] Space Telescopes Science Institute 2022, Available at: https://jwst-docs.stsci.edu/jwst-mid-infrared-instrument/miri-observing-modes/miri-imaging

[2] Space Telescopes Science Institute 2022, Available at: https://jwst-docs.stsci.edu/jwst-near-infrared-camera

[3] Space Telescopes Science Institute 2022, Available at: https://jwst-docs.stsci.edu/jwst-near-infrared-imager-and-slitless-spectrograph

[4] Space Telescopes Science Institute 2022, Available at: https://jwst-docs.stsci.edu/jwst-near-infrared-spectrograph

NIRISS is one of JWST's imager/spectrograph instruments. (Space Telescope Science Institute 2020). The NIRISS instrument will observe wavelengths in the NIR spectrum (0.6 to 5.0 µm) and has four observation modes; the wide field slitless spectroscopy (WFSS), single object slitless spectroscopy (SOSS), aperture masking interferometry (AMI) and imaging (Space Telescope Science Institute 2022c). NIRISS will be used to characterise exoplanet atmospheres and observe the spectrums of transiting exoplanet (NASA 2022a).

2.3.3.2 Capabilities and Future Outcomes of JWST

Bean, JL et al. (2018) predicts that the JWST will be able to observe the atmospheric compositions of transiting exoplanets, which is a fact supported by the known capabilities of the JWST instruments. The JWST instruments will primarily observe in the infrared spectrum where, across its four instruments, covers the range of wavelengths between 0.6 to 28 µm (ICNIRP 2020). The molecules (and their associated isotopes) that can be detected within this wavelength range, with a strong signal, include CO_2 ($^{12}C^{16}O_2$), CH_4 ($^{12}CH_4$), SO_2 ($^{32}S^{16}O_2$), N_2 ($^{14}N_2$), O_3 ($^{16}O_3$), CO ($^{12}C^{16}O$), and NH_3 ($^{14}NH_3$) (Gordon et al. 2022). These molecules cannot be detected by the HST since it observes wavelengths between 0.115 and 1.7 µm. As per section 2.3.1 – *Capabilities and Limitations of HST*, the isotopes listed with these molecules are the most abundant within this wavelength range. Further information about these isotopes can be found in the HITRAN database (Gordon et al. 2022).Figure 5shows the capabilities expected of the JWST instruments (Bean, J. et al. 2018). Bean, J. et al. (2018) used a program called PandExo to develop simulated observations of WASP-79b which was compared to existing data of WASP-79b collected by the HST

WFC3 instrument. From Figure 5, the simulated observations show that JWST will be able to observe strong molecular signals of H_2O, CO and CO_2 whereas HST is limited to only detecting weak molecular signals of H_2O (Bean, J. et al. 2018). Compared to Figure 4 which depicts observation data of the TRAPPIST-1 system collected by the HST WFC3 instrument, the resolution of detectable molecules of the JWST instruments are also superior to that of the HST instruments.

Since infrared wavelengths are longer than other wavelengths such as the optical and UV, the JWST instruments will be able to make observations that will not be interfered by dust and cloud. This means that the instruments on board the JWST will also be able to detect fainter and more distant objects such as small terrestrial exoplanets (Barstow et al. 2015).

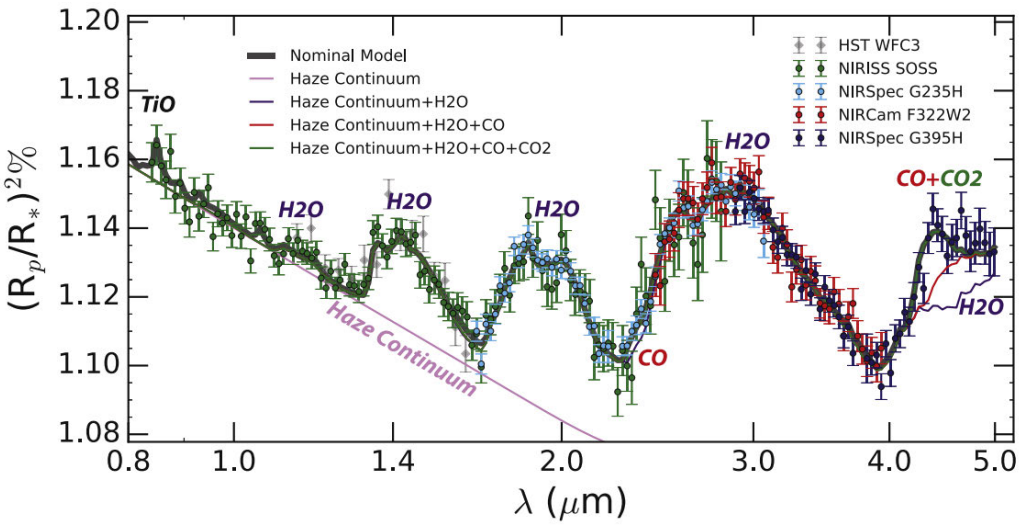

Figure 5: Simulated transmission spectral data of WASP-79b expected to be observed by the JWST instruments (NIRISS, NIRSpec and NIRCam) using the program, PandExo. The simulated data is plotted with the observed transmission spectral data of WASP-79b collected by the HST WFC3 instrument. The plot also depicts the molecules for each transmission peak. These molecules include H_2O, CO and CO_2. Sourced from Bean, J. et al. (2018).

The molecules that JWST can detect are also expected to be observed in the atmospheres of Venus-like exoplanets which may confirm their existence in the universe. JWST will also be able to detect these molecules at longer, more abundant wavelengths, therefore it will be easier to characterise the atmospheres of Venus-like exoplanets. The data collected by JWST, including the atmospheres of Venus-like exoplanets, will be available to the public in databases such as the NASA Exoplanet Archive.

2.4 Database Archive

As stated in section 1.1, the search for Venus-like exoplanets may assist the future characterisation of terrestrial exoplanets. To identify a Venus-like exoplanet, the atmospheric composition of confirmed exoplanets found in nearby planetary systems would need to be compared to that of modern Venus. To determine the transmission absorption spectrum and the atmospheric composition of the Venus-like candidates, the Python programs PLATON and TauREx will be used to simulate this using the astrophysical parameters of exoplanets and model their atmospheric characteristics (see section 2.5). These parameters can be found by searching databases containing the data collected by space-based observatories. In this project, the NASA Exoplanet Archive will be used to find exoplanets orbiting solar analogs that have similar planetary specifications to Venus, specifically its mass, radius and orbital semi-major axis (i.e. the planet's proximity to its host star).

The NASA Exoplanet Archive contains astronomical data on exoplanets from many astronomical data collections (NASA Exoplanet Science Institute 2021b). The data

provided in this archive is collected from the Kepler, TESS and CoRot missions, along with many ground-based surveys (Akeson et al. 2013). This archive allows users to search for specific exoplanet parameters including planet mass, radius, orbital period, and isothermal temperature. It also allows users to find specific stellar parameters such as the star mass, radius and temperatures (NASA Exoplanet Science Institute 2021b).

2.5 Simulation programs

With the launch of JWST, data of Venus- and Earth-like exoplanets are expected to be collected and uploaded to the NASA Exoplanet Archive. Because the JWST data will not be available to the public for some time, researchers have been using programs such as PLATON and TauREx to simulate what we expect to find from the JWST mission.

2.5.1 PLATON

Planetary **A**tmosperic **T**ool for **O**bserver **N**oobs (PLATON) is a Python package that can calculate and model simple transmission absorption and emission spectra of exoplanets, as well as calculate their atmospheric properties (Zhang et al. 2019). PLATON has three main modules: TransitDepthCalculator, EclipseDepthCalculator and CombinedRetriever. For this project, only the TransitDepthCalculator will be used to model the transmission absorption spectra of Venus and the Venus-like candidates.

TransitDepthCalculator is used to compute the transmission absorption spectrum of transiting exoplanets (Zhang et al. 2019). The calculations for this module require the user to input parameters of the planetary system being modelled such as the star's radius, the planet's radius, the planet's mass, and the isothermal temperature of the planet's atmosphere. The models also consider other atmospheric parameters of the exoplanet such as the absorption of gas in the atmosphere, collision-induced absorption (Akeson et al.), Rayleigh and Mie scattering, as well as the effects of clouds (Zhang et al. 2019). The module then outputs both the plot and tabulated data of the wavelength versus the transit depth. By plotting the transit depths against the wavelengths, the transmission absorption spectrum of the exoplanet's atmosphere is modelled (Zhang et al. 2019). A detailed description of the TransitDepthCalculator in PLATON can be found in Appendix C.1.

Zhang et al. (2020) used the capabilities of PLATON to model the transmission and emission spectra of the hot Jupiter exoplanet known as HD 189733b. These models were then compared to the available data collected by HST and Spitzer (Zhang et al. 2020). The models developed by Zhang et al. (2020) were the first comprehensive models of HD 189733b. They found that there were distinct similarities between the models and the spectra observed by HST and Spitzer, demonstrating the accuracy of PLATON's algorithm (Zhang et al. 2020).

2.5.2 TauREx

The Tau Retrieval for Exoplanets (TauREx) is a Python code predominantly used for analysing the atmospheres of gas giant exoplanets. However, the updated TauREx III

now allows users to model the atmospheres of relatively smaller and colder exoplanets such as terrestrials (Al-Refaie et al. 2021). In this thesis, TauREx III will be referred to as TauREx. The code requires an input of the transmission absorption spectral data of the exoplanet's atmospheres. This can be either data collected from space-based observatories or modelled spectral data (Barstow et al. 2020). The user must also input the exoplanet's mass, radius, and isothermal temperature. The chemistry of the planet's atmosphere can be modified by altering the presence and abundance of molecules in the atmosphere (Barstow et al. 2020). This means that users can then model the atmosphere to fit the observational data and confirm the presence of molecular species in the planet's atmosphere (Barstow et al. 2020). This helps the user identify which molecules contribute to the absorption of light in the atmosphere (i.e. active molecules) or interact with the incoming light and other molecules in the atmosphere (i.e. inactive molecules). This includes molecules that contribute to Rayleigh Scattering in the atmosphere (Al-Refaie et al. 2021). For more detail on the use of the TauREx code, see Appendix C.2.

TauREx has been extensively used for projects specific to the characterisation of exoplanet atmospheres, more specifically the atmospheres of Jovian exoplanets. In 2021, Tsiaras et al. (2021) presented their work on detecting water vapour in the atmosphere of K2-18b. This was achieved by using the data collected by HST's WFC3 instrument which collected eight transit observations of K2-18b. The raw observation data was then analysed through TauREx to determine the atmospheric parameters. From this, Tsiaras et al. (2021) modelled three different atmospheric scenarios for K2-18b: two different cloud-free atmospheres (H_2O only, and H_2O + N_2) and a cloudy atmosphere (H_2O + clouds). Although three different scenarios were presented, all

models showed the presence of water vapour. In addition, there was no significant difference found between the $H_2O + N_2$ cloud-free model and the H_2O + clouds model at a 2σ uncertainty range (Tsiaras et al. 2021). Limitations of the model that were identified by Tsiaras et al. (2021) include the inability to identify other molecules in the atmosphere due to the signal-to-noise ratio and the wavelength coverage of the HST's WFC3 instrument. Taking these findings into consideration, the Venus-like candidates in this project will only be modelled as a cloud-free atmosphere since the application of a cloudy atmosphere is unlikely to present significantly different results to the cloud-free spectral output of relatively small terrestrial exoplanets.

2.6 The Importance of Terrestrial Exoplanet Characterisation

Currently, the method for the classification of terrestrial exoplanets is flawed since the differences in atmospheric characteristics are indistinguishable with our current instrumentation. This means that most terrestrial exoplanets are often classified as 'Earth-like' or 'super-Earth' exoplanets without due consideration of the known differences between the terrestrial planets within our solar system. Since this is the current method for classifying terrestrial exoplanets, a terrestrial exoplanet with Venus-like characteristics may be classed as an Earth-like exoplanet. To refine this classification, the specific characteristics of terrestrial exoplanet atmospheres must be identified. This can then be applied when space-based instrumentation is able to make the distinction between Earth-like and Venus-like exoplanets.

This project is expected to expand on our current knowledge of Venus-like exoplanet atmospheres through simulations which can help guide future space-based instrumentation, with improved capabilities, in the search for planetary systems like our own.

CHAPTER 3: AIMS AND RESEARCH QUESTIONS

There are many confirmed terrestrial candidates residing in planetary systems that may exhibit similar geophysical properties to our solar system's terrestrial planets, like Earth and Venus. However, due to the observational and technological limitations with our current space telescope instruments, this number is likely to represent the existence of only a small fraction of these types of exoplanets. These limitations include observation time, instrument lifetime, and capabilities, which combined, result in a reduction in the likelihood of successfully characterising relatively small, terrestrial exoplanets.

As the classification of terrestrial exoplanets becomes more refined upon the discovery of new exoplanets, this knowledge, in conjunction with sophisticated models, can be used to further refine the parameters of specific exoplanet candidates. Chapter 2 prefaced that, although the HST instrumentation was state-of-the-art for its time, a wider wavelength range is required to characterise the molecular species contained with exoplanetary atmospheres. Thus, future research of exoplanet atmospheres will eventually lead to the improved classification of terrestrial exoplanets. Possible candidates that could assist the classification of terrestrial exoplanets are Venus-like exoplanets. As planned space-based instruments mostly use the infrared spectrum, the molecules of a Venus-like exoplanet will be easier to detect. This would be a first step into accurately characterising exoplanet atmospheres and therefore, can contribute to the improved classification of terrestrial exoplanets.

3.1 Research Questions

With the information from the previous section in mind, the research questions of this project are:

1. Can atmospheric simulations of Venus and Venus-like candidates be used to guide the detection of molecular species and key properties of Venus-like exoplanets, using the next generation of space-based observatories?
2. Can these simulations also be used to refine the classification of terrestrial exoplanets, particularly Earth- and Venus-like exoplanets, and assist our understanding of exoplanet and planetary system evolution?

CHAPTER 4: METHODOLOGY

The aim of this project is to identify Venus-like exoplanets orbiting solar analogs using the NASA Exoplanet Archive. Since the HST instruments do not have the capability of detecting molecules expected to be found in the atmospheres of Venus-like exoplanets, the Python program, PLATON will be used to model the expected transmission absorption spectra of Venus and the Venus-like candidates that will be observed by the JWST. From this, the modelled spectral data from PLATON will then be inputted into the Python program, TauREx, to characterise the atmospheres of the Venus-like candidates. The models of the Venus-like candidate's atmospheres will also be compared to the TauREx model of the Venus atmosphere, where any similarities and differences between the models and to real instrumentation capabilities will be identified. This will lead to the discussion of the likelihood that the candidates are Venus-like and further explore other possible inferences such as the evolutionary status of the planetary system. This method will also determine whether current space-based observatories and future missions will be capable of detecting Venus-like exoplanets.

4.1 Data Collection

The NASA Exoplanet Archive was used to search for Venus-like candidates. That is, exoplanets with similar astrophysical characteristics to Venus. The NASA Exoplanet Archive allows users to specify parameters for the exoplanet and the star.

To find the Venus-like candidates, each parameter was individually refined until exoplanets with astrophysical characteristics most similar to Venus were found.

Table 6: The astrophysical specifications of Venus including its mass in Earth masses (M_{Earth}), radius in Earth radii (R_{Earth}), and orbital semi-major axis in au. Modified from California Institute of Technology (2019).

Planetary Parameter	Value
Mass	0.815 M_{Earth}
Radius	0.950 R_{Earth}
Orbital semi-major axis	0.723 au
Planet Density	5.2 g/cm^3

First, the star type was specified, narrowing the search to only include systems containing solar analogs.

From the list of exoplanets produced, the search was further refined to only include terrestrial exoplanets. That is, exoplanets located within the TZ or VZ, that also have a mass, radius, and planet density similar to Venus (refer to Table 6 for the values used for these parameters). The exoplanets identified to be most Venus-like were tabulated to form the list of Venus-like candidates.

4.2 Python Programs Installation

The installation of PLATON and TauREx were completed on a Mac Operating System (OS). The specifications of the device used to install these packages can be found in Appendix A. The online installation guide for PLATON (Zhang et al. 2019) and TauREx (Al-Refaie et al. 2021) were used to install the software. An overview of the installation process used for these packages can be found in Appendix B.

4.3 PLATON Planetary Spectral Models

For this project, PLATON's TransitDepthCalculator template from the PLATON documentation was used to model the transmission absorption spectra of Venus and the Venus-like candidates (see Appendix C.1 for details about the PLATON code). Note that this code was modified and run in Jupyter Notebooks. PLATON's TransitDepthCalculator required the user to input the planet and star's parameters. This included the planet's radius, mass, and isothermal temperature as well as the star's radius, mass, and temperature. The PLATON code was then run to output the spectra of each of the planet. The format in which the spectra was outputted into includes a data file (.dat file extension) as well as an image of the spectral plot (.jpg file extension).

For the PLATON output to be suitable for the TauREx input, modifications to the PLATON code had to be made. To input a data file into TauREx, it needs to be a three-column ASCII file where the three columns are the exoplanet's wavelength, the transit depth, and the standard error. The standard error is used to determine the accuracy of the simulated data. The first two columns (wavelength and transit depth) were calculations that the PLATON code originally produced. However, PLATON does not compute the standard error. The calculations for the standard error needed to be incorporated into the code and outputted as the third column. This was achieved by creating an array of the standard error, which was then combined into the original two column output of PLATON. For the modifications made to the PLATON code, see Appendix C.1.

Initially, the JWST Exposure Time Calculator (JWST ETC) (Pontoppidan et al. 2016) would be used to calculate the signal-to-noise ratio (SNR) of each exoplanet's simulated transmission absorption spectrum. However, the SNR calculated by the JWST ETC only accounts for specific instruments on JWST and some HST instruments. To ensure that the simulations could be compared to a range of instruments, an inflated standard error of two times the calculated standard error was used. According to Tsiaras et al. (2021), a 2σ uncertainty range provided a significant overlap between a cloudy and cloud-free atmosphere. This is used here to ensure that the model incapsulated all scenarios. To calculate the new standard error, the following Python equation was incorporated (The SciPy community 2022):

$$2 \times Standard\ Error = \frac{2\sigma}{\sqrt{n}}$$

Where 2σ is the standard deviation of the sample as given by Tsiaras et al. (2021), and n is the sample size which, in this case, is number of data points plotted by PLATON. The value for n for all PLATON outputs is 461. The resulting standard error is therefore two times the standard error.

It is acknowledged that the JWST Exposure Time Calculator (Pontoppidan et al. 2016) signal-to-noise ratio values are more accurate however, the inflated standard error was used instead due to the formatting required by TauREx. The inflated standard error is still a good indication of the estimated average SNR of the PLATON data. If this research is pursued further, the SNR should be incorporated to determine a more accurate error.

Here, TRAPPIST-1b is used as an example of an SNR modelled by the JWST ETC. The SNR is calculated at each individual wavelength data point. The PLATON simulation for TRAPPIST-1b computes and outputs the dataset of its wavelengths and corresponding transit depths. The outputted .dat file is then inputted into the JWST ETC which plots the spectrum's SNR (see Figure 4). Figure 4 clearly shows that the SNR changes with wavelength, therefore would be more accurate than the use of a standard error which is averaged over all wavelengths. Thus, reaffirming the need for this to be incorporated in future models for JWST simulations.

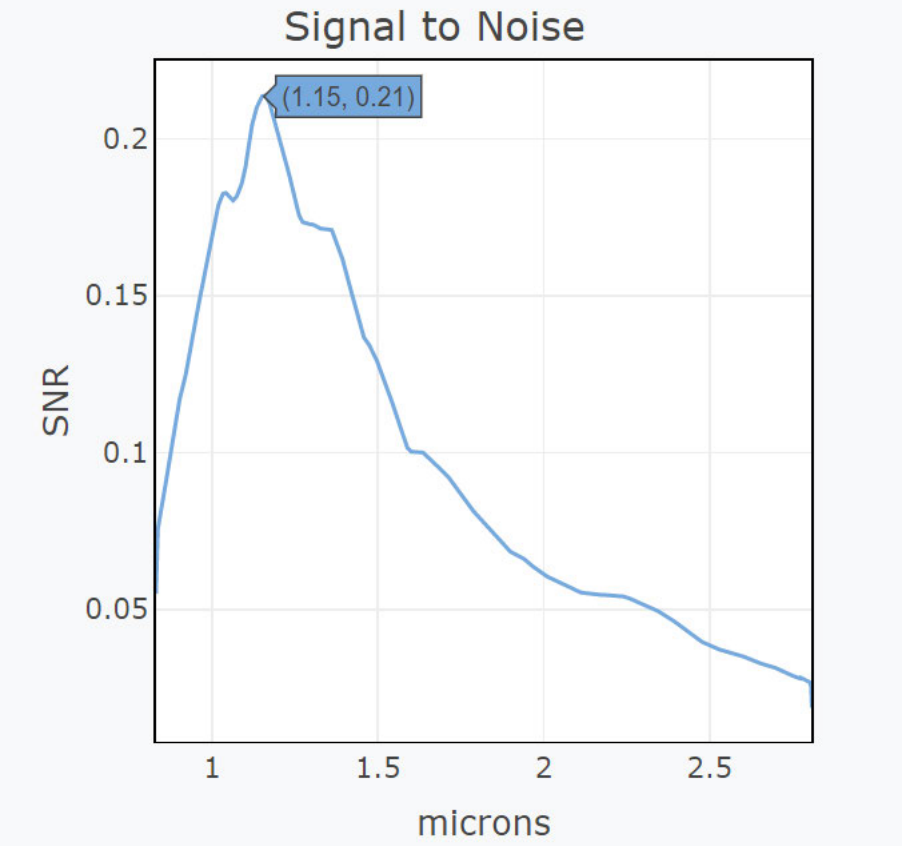

Figure 6: Plot of the TRAPPIST-1b signal-to-noise ratio (SNR) using the JWST Exposure Time Calculator (JWST ETC) (Pontoppidan et al. 2016). The x-axis represents the wavelength in microns (µm), and the y-axis represents the corresponding SNR. The peak of the plot is the maximum SNR. For TRAPPIST-1b, the maximum SNR is 0.21 at 1.15 µm.

4.4 Characterisation of Planet Atmospheres using TauREx

TauREx was used to model the atmospheres of Venus and the Venus-like candidates. The TauREx code was run using a simple .par file which contained modifiable parameters for the planet being modelled. This includes the planet's astrophysical parameters as well as the star's parameters. The modelled data of the transmission absorption spectra for each planet was inputted into the .par file. This was achieved by setting the path to the folder that contained the .dat file for the planet being modelled.

The parameters for the planet and star were set to match the data found in the NASA Exoplanet Archive. The planetary parameters set in the .par file are the planet's radius, mass, semi-major axis, orbital period and isothermal temperature. The user can also set the pressure profile of the planet however, it was later determined that it was best to keep this parameter as the default. The star parameters set in the .par file are the star's radius, mass and temperature. The user can also include the star's metallicity however, it was later determined that this does not significantly change the outcome of atmospheric retrieval. Once these parameters were set, the chemistry of the planet's atmosphere could now be modified. In TauREx, the user is able to modify the active and inactive molecules present in the model. The active molecules available in TauREx include CH_4, NH_3, CO_2, H_2O and CO. The inactive molecules available in TauREx include He, H_2, O_2 and N_2. For this project, the opacity file for SO_2 was downloaded from the HITRAN repository (Gordon et al. 2022).

To determine which molecules were likely to be found in the planet's atmosphere, the process of elimination was incorporated to see which molecules allowed the

model to fit the data. Each molecule available in TauREx was set as the fill gas to see which one best fit within the uncertainties of the observation, where possible. The molecules that aligned with the observation were added to the list of possible molecules present in the planet's atmosphere. Once the active molecules likely to be present were determined, the fill gas was replaced with inactive molecules. Since the planet's being modelled in this project are likely terrestrial, He and N_2 were predominantly used as fill gases. Through systematic reiteration, the abundance of each molecule was modified until the model converged on the observations.

The .par file was then run through the Mac terminal to plot the forward model and the observation together (see Appendix C.2 for the commands used). The contributions of individual molecules, including the contributions of Rayleigh Scattering, were also plotted. This allowed the user to distinguish which molecules affected the transmission absorption spectra of the atmosphere. The transmission absorption models of the Venus-like candidates will then be compared to real instrumentation capabilities of HST and JWST to determine if the molecules expected to be in their atmospheres are detectable now and in the future.

CHAPTER 5: RESULTS

5.1 Collection of Exoplanet Data

The specifications of Venus (see Table 6) along with the classification of solar analogs (see section 2.1.1) have been used to find candidates for Venus-like exoplanets. An extensive search of the NASA Exoplanet Archive was conducted to find exoplanets with similar astrophysical parameters to Venus. From this search, a list of 23 potential Venus-like candidates were found (see Table 7). This search was then narrowed to determine which exoplanets had the available parameters required for the PLATON input (e.g. the planet's isothermal temperature) to simulate the Venus-like candidate's transmission absorption spectrums (see Table 8). The top four exoplanet candidates were chosen to be modelled in PLATON and TauREx. The final five candidates chosen, including Venus, were TRAPPIST-1b, TRAPPIST-1c, GJ 9827c, and Kepler138c (see Section 5.2). These exoplanets were selected mostly from different planetary systems to diversify the samples modelled in PLATON and TauREx. TRAPPIST-1b and -1c were chosen to compare exoplanets within the same planetary system. Table 8 contains the final list of Venus-like candidates, where the planets with an asterisks were modelled in PLATON and TauREx.

Table 7: Exoplanets and their astrophysical parameters found using the NASA Exoplanet Archive. The exoplanets are ranked in order of most to least similar astrophysical characteristics to Venus. This table also includes comments on the appropriateness of the exoplanet in terms of its similarities to Venus as well as any information on the exoplanet in associated journal articles found in the databases. Modified from Space Telescope Science Institute (2021) and NASA Exoplanet Science Institute (2021a).

Rank	Star Name	Planet Name	Planet Mass (M_{Earth})	Planet Density (g/cm^3)	Planet Radius (R_{Earth})	Orbital semi-major axis (au)	Spectral type	Orbital Period (Days)	Distance to Host Star (pc)
1	TRAPPIST-1	TRAPPIST-1b	0.850	3.6±3.1	1.086	0.01111	M8 V	1.51087081	12.098491
2	TRAPPIST-1	TRAPPIST-1f	1.039	5.02	1.045	0.03849	M8 V	9.207540	12.098491
3	TRAPPIST-1	TRAPPIST-1g	1.321	5.06	1.129	0.04683	M8 V	12.352446	12.098491
4	TRAPPIST-1	TRAPPIST-1e	0.62±0.58	4.4±4.2	0.918	0.02817	M8 V	6.099615	12.098491
5	TRAPPIST-1	TRAPPIST-1d	0.388	4.37	0.788	0.02227	M8 V	4.049219	12.098491
6	TRAPPIST-1	TRAPPIST-1h	0.326	4.16	0.755	0.06189	M8 V	18.772866	12.098491
7	TRAPPIST-1	TRAPPIST-1c	1.38	6.45±2.92	1.056	0.01521	M8 V	2.4218233	12.098491
8	GJ 9827	GJ 9827c	2.42	4.13	1.24	0.0429	K6 V	3.64823	29.6610
9	TOI-561	TOI-561 b	1.59	3.0	1.423	0.01055	G9 V	0.446578	85.7990
10	GJ 581	GJ 581 e	1.7	-	-	0.028453	M3 V	3.14867	6.2981
11	GJ 9827	GJ 9827d	2.35	1.51	2.10	0.060	K6 V	6.20141	29.6610

Rank	Star Name	Planet Name	Planet Mass (M_{Earth})	Planet Density (g/cm^3)	Planet Radius (R_{Earth})	Orbital semi-major axis (au)	Spectral type	Orbital Period (Days)	Distance to Host Star (pc)
12	GJ 9827	GJ 9827c	2.42	6.4	1.269	0.03942	K5 V	3.648083	29.6610
13	GJ 48n6	GJ 486 b	2.82	7.0	1.305	0.01734	M3.5 V	1.467199	8.07426
14	L98-59	L98-59 e	3.06	-	-	0.0717	M3 V	12.796	10.6194
15	GJ 9827	GJ 9827b	3.42	4.5	1.62	0.01888	K5 V	1.2089802	11.2810
16	HD 40307	HD 40307 f	3.63	-	-	0.2485	K3 V	51.56	12.9363
17	GJ 9827	GJ 9827b	3.69	5.11	1.58	0.0206	K6 V	1.208966	29.6610
18	HD 40307	HD 40307 b	3.81	-	-	0.0475	K3 V	4.3115	12.9363
19	Kepler-138	Kepler-138c	3.83	5.0	1.61	-	M1 V	13.78164	66.8624
20	HD 3167	HD 3167 b	5.02	5.60	1.70	0.01815	K0 V	0.959641	47.2899
21	61 Vir	61 Vir b	5.1	-	-	0.050201	G5 V	4.12150	8.50332
22	K2-141	K2-141b	5.31	8.00	1.54	0.716	K7 V	0.2803266	61.8736
23	GJ 581	GJ 581 c	5.6	-	-	0.072993	M3 V	12.9191	6.2981

Table 8: Venus and exoplanet parameters used to simulate the transmission absorption spectra in PLATON. The exoplanets in this table were derived from Table 7, where only the exoplanets listed here had the data required for the PLATON input. The information given in this table is specific to the PLATON simulations, including the units for each parameter. Modified from NASA Exoplanet Science Institute (2021a).

Planet Name	Star Radius (R_{solar})	Star Mass (M_{solar})	Star Temperature (K)	Star Age (Gya)	Planet Mass (M_{Jup})	Planet Radius (R_{Jup})	Planet Distance (au)	Orbital Period (days)	Isothermal temperature (K)
Venus*	1.00000	1.0000	5778	4.5	0.02564	0.08465	0.723	225	260
TRAPPIST-1b*	0.11920 ±0.0013	0.0898 ±0.0023	2556±26	>0.5	0.00432 ±0.069	0.0969 ±0.00125	0.01154 ±0.0001	1.51 ±0.000006	400 ± 9
TRAPPIST-1f	0.11920 ±0.0013	0.0898 ±0.0023	2556±26	>0.5	0.00327 ±0.000098	0.0932 ±0.00116	0.03849 ±0.00033	9.21 ±0.000032	219±4.2
TRAPPIST-1e	0.11920 ±0.0013	0.0898 ±0.0023	2556±26	>0.5	0.00218 ±0.00007	0.0821 ±0.0012	0.02925 ±0.0025	6.10 ±0.000035	251±4.9
TRAPPIST-1d	0.11920 ±0.0013	0.0898 ±0.0023	2556±26	>0.5	0.00122 ±0.00004	0.0703 ±0.001	0.02227 ±0.00019	4.05 ±0.000026	288±5.6
TRAPPIST-1c*	0.11920 ±0.0013	0.0898 ±0.0023	2556±26	>0.5	0.00412 ±0.000176	0.0979 ±0.00125	0.0158 ±0.00013	2.42 ±0.000018	342±6.6
GJ 9827c*	0.61300 ±0.06	0.606 ±0.07	4199±125	10	0.00761 ±0.002	0.1132 ±0.007	0.03925 ±0.0006	3.65 ±0.00006	811±30

Planet Name	Star Radius (R_{solar})	Star Mass (M_{solar})	Star Temperature (K)	Star Age (Gya)	Planet Mass (M_{Jup})	Planet Radius (R_{Jup})	Planet Distance (au)	Orbital Period (days)	Isothermal temperature (K)
GJ 9827d	0.61300 ±0.06	0.606 ±0.07	4199±125	10	0.01270 ±0.0026	0.1804 ±0.004	0.05591 ±0.0005	6.20 ±0.00006	646±20
GJ 486b	0.32300 ±0.011	0.323 ±0.015	3340±54	-	0.00887 ±0.00035	0.1164 ±0.0058	0.01734 ±0.00026	1.47 ±0.00003	701±13
GJ 9827b	0.61300 ±0.06	0.606 ±0.07	4199±125	10	0.01540 ±0.0015	0.1407 ±0.0026	0.0188 ±0.00018	1.21 ±0.000007	1114±36
Kepler-138c*	0.54399 ±0.0158449	0.5398 ±0.02375	3880±157	4.7	0.00619 ±0.006	0.1068 ±0.0062	0.0922 ±0.004	13.8 ±0.0001	398
HD 3167b	0.88197 ±0.0629	0.91 ±0.1	5438±63	5	0.0176 ±0.003	0.143 ±0.008	0.0186 ±0.0003	0.959 ±0.000044	531

* Planets selected to be modelled in PLATON and TauREx

Table 9: Fraction of molecular species present in the Venus-like candidates in TauREx models. As seen by the fractions given in the table, these values do not equal one, and are not required to (section 2.5.3). The TauREx code determines the remainder of the molecular species fractions in the atmosphere.

	Modern Venus	**Ancient Venus**	**TRAPPIST-1b**	**TRAPPIST-1c**	**GJ 9827c**	**Kepler 138c**
Fill gas ratio [gas-1, gas-0]	[CO_2, N_2] 0.0363	[He, N_2] 0.009	[He, N_2] 0.001	[He, N_2] 0.0001	[He, N_2] 0.01	[He, N_2] 0.001
Absorption CO_2	-	-	-	-	-	-
Absorption SO_2	0.00015	-	-	-	0.000035	-
Absorption H_2O	0.00002	0.0005	0.0006	0.0001	0.0015	0.002
Absorption CO	0.000017	-	-	-	-	-
Absorption CH_4	-	0.005	0.009	0.0007	0.0007	0.007
Absorption NH_3	-	0.009	0.0005	0.00009	-	0.004

5.2 Atmospheric Models in PLATON and TauREx

The following transmission absorption spectrums (i.e. the transit depth vs. wavelength) were modelled using the Python code, TauREx (section 4.4) where the observation for each of exoplanet was simulated in PLATON as outlined in section 4.3. The observations were then used as an input into TauREx, where the forward model could then be matched to the observation. A detailed description of how to use TauREx can be found in Appendix C.2.

Table 9 contains the fraction of the molecular species used to model the Venus-like candidates in TauREx. Seen here, the fractions do not equal one since the code determines the remainder of the fraction of the molecular species. Trials were run to

confirm this by forcing the fractions to equal one. However, it was found that the model would not converge to the observations better than the values listed in Table 9. This is supported by section 2.5.3.

The transmission absorption spectrum of modern Venus was modelled in TauREx using the known molecular species present in the modern Venus atmosphere (Figure 7a). This atmosphere contains a high abundance of CO_2 and N_2, with traces of H_2O, Ar and SO_2. The percentages of the molecules present in modern Venus' atmosphere can be found in Table 1. In Figure 7b, the transmission absorption spectrum of modern Venus was also simulated in PLATON using the known Venus astrophysical parameters and then plotted against the model of the modern Venus atmosphere (see Table 8). It is apparent that the model and the simulation do not match. This is because the modern Venus atmosphere displays characteristics of volcanic outgassing and the runaway greenhouse effect. Such factors cannot be accounted for in PLATON, therefore, the PLATON simulations are more similar to that of an Ancient Venus atmosphere prior to volcanic outgassing and the runaway greenhouse effect. Figure 7c shows how each molecule contributes to the absorption of light in modern Venus' atmosphere. Active molecules present such as CO_2, SO_2 and H_2O contribute to atmospheric absorption. CO_2 is the highest absorber in modern Venus' atmosphere. High CO_2 absorption occurs at ~1.8, 3.2 and 10.7 μm. Although SO_2 is only a trace gas in modern Venus' atmosphere, it also contributes to a large amount of absorption which occurs at ~7.0, 9.0 and 11.0 μm. Unlike CO_2 and SO_2, H_2O has a small contribution to absorption at ~5.0 and ~12.0 μm. Inactive gases like He and N_2 contribute only to the effects of Rayleigh Scattering in modern Venus' atmosphere.

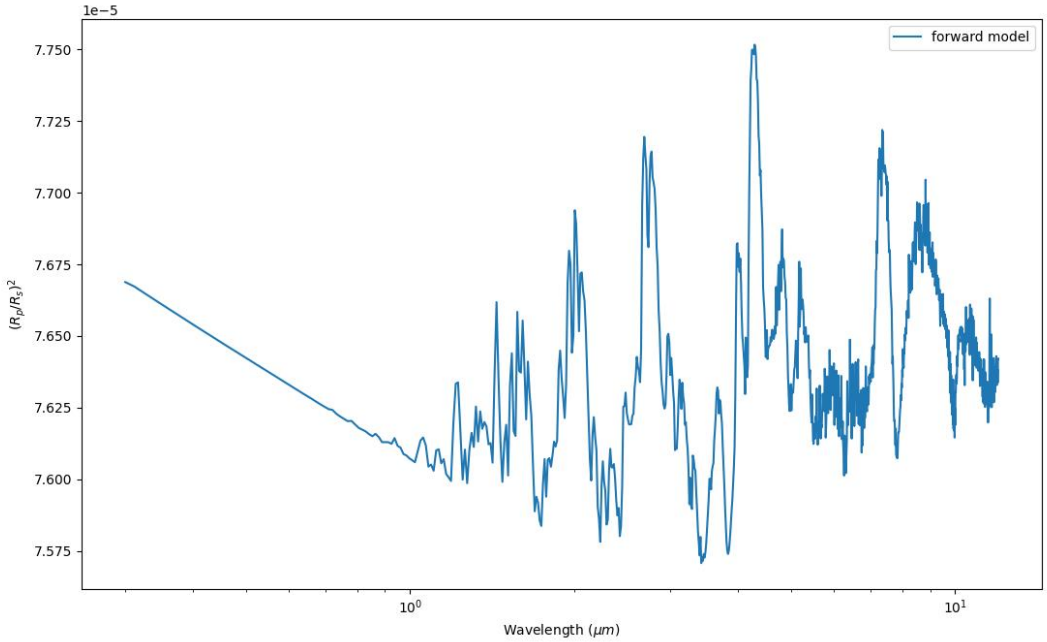

Figure 7a: Plot of the forward model of the modern Venus transmission absorption spectrum in TauREx using the **known** abundance of each molecular species in Venus' atmosphere (see Table 1). The x-axis represents the wavelength in microns (µm) as a logarithmic scale, and the y-axis represents the transit depth $((R_p/R_s)^2) \times 10^{-5}$.

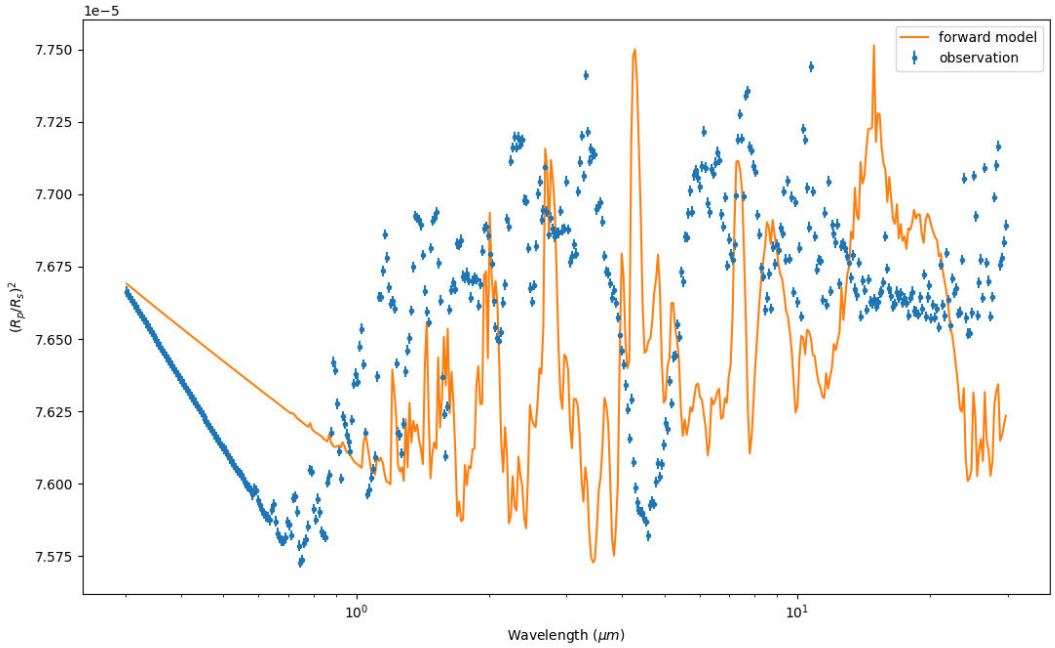

Figure 7b: Plot of the forward model of the Venus transmission absorption spectrum in TauREx using the **known** abundance of each molecular species in Venus' atmosphere (orange line) versus the simulated transmission absorption spectrum of Venus from PLATON (blue dots). The x-axis represents the wavelength in microns (µm) as a logarithmic scale, and the y-axis represents the transit depth $((R_p/R_s)^2) \times 10^{-5}$.

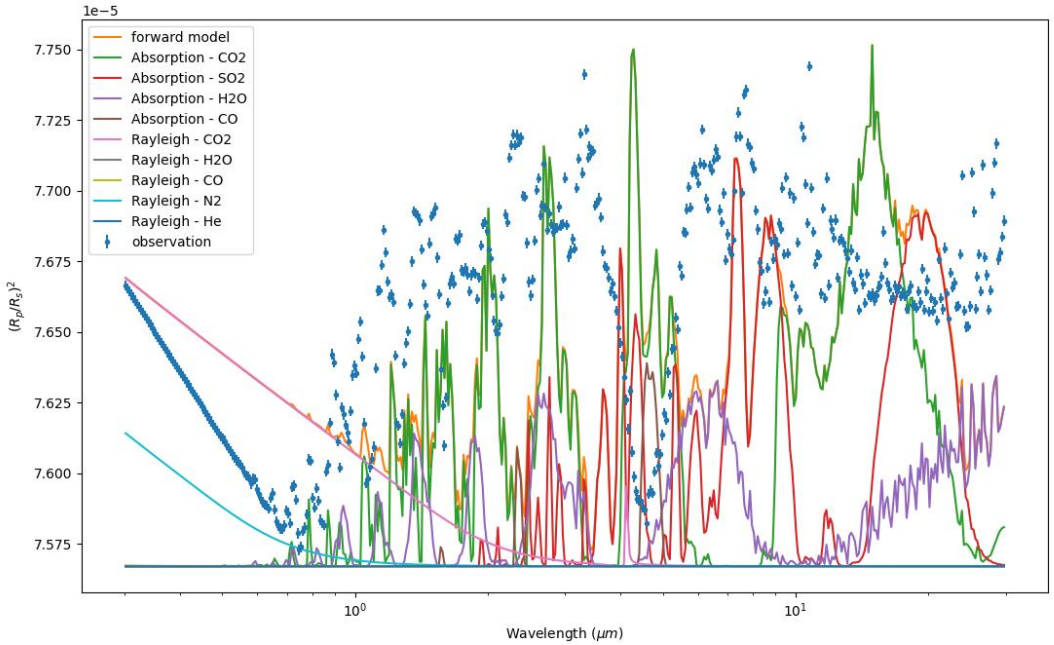

Figure 7c: Plot of the forward model of the Venus transmission absorption spectrum in TauREx using the known abundance of each molecular species in Venus' atmosphere (orange line) versus the simulated transmission absorption spectrum of Venus from PLATON (blue dots) where the x-axis represents the wavelength in microns (µm) as a logarithmic scale, and the y-axis represents the transit depth $((R_p/R_s)^2) \times 10^{-5}$. This plot also contains the individual plots of each molecule's contribution to the planet's modelled transmission absorption spectrum. This includes plots of the individual active and inactive molecules that affect the overall spectral output. For this model, the active molecules are CO_2, SO_2, H_2O and CO. The inactive molecules that contribute to the effects of Rayleigh Scattering are N_2 and He.

The simulated transmission absorption spectrum created in PLATON was modelled using TauREx to compare the simulated to the known characteristics of the Venus atmosphere (Figure 8a). It was determined that the simulated Venus atmosphere contains the active molecules CH_4, NH_3 and H_2O, which contribute to the absorption of light in the atmosphere. The simulated Venus atmosphere also contains traces of inactive molecules N_2 and He, which contribute to the effects of Rayleigh Scattering in the atmosphere (Figure 8b). Because the PLATON simulation does not account for volcanic outgassing and the runaway greenhouse effect, this model is more

comparable to models of the Ancient Venus atmosphere, which is an atmosphere that lacks greenhouse gases and thick cloud layers.

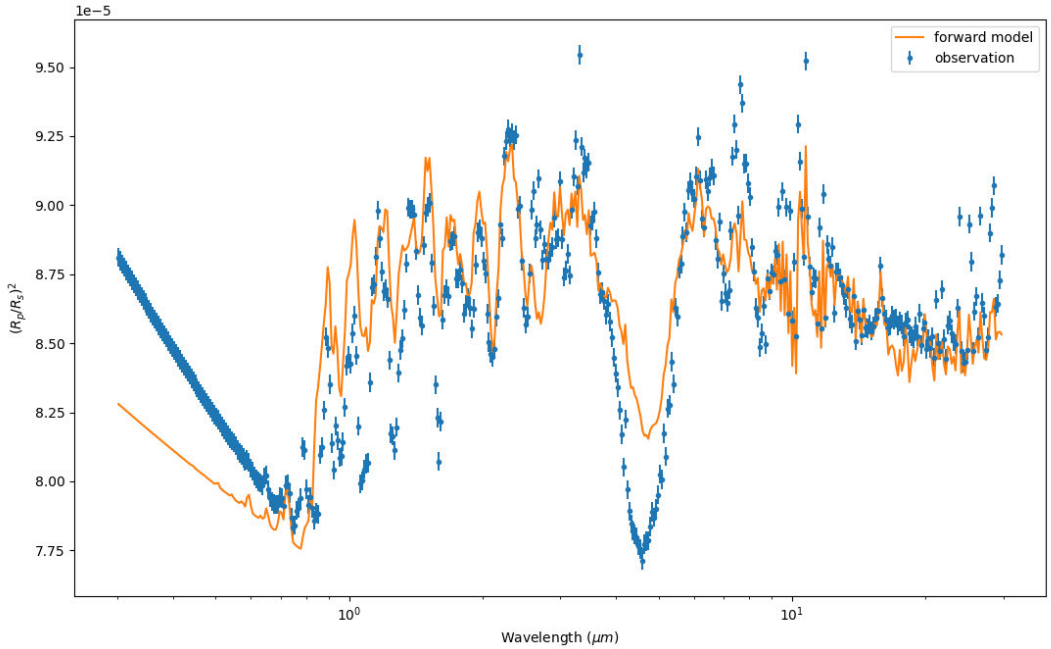

Figure 8a: Plot of the forward model of the Ancient Venus transmission absorption spectrum in TauREx (orange line) against the transmission absorption spectrum simulated in PLATON (blue dots). The x-axis represents the wavelength in microns (µm) as a logarithmic scale, and the y-axis represents the transit depth ($(R_p/R_s)^2$) × 10^{-5}.

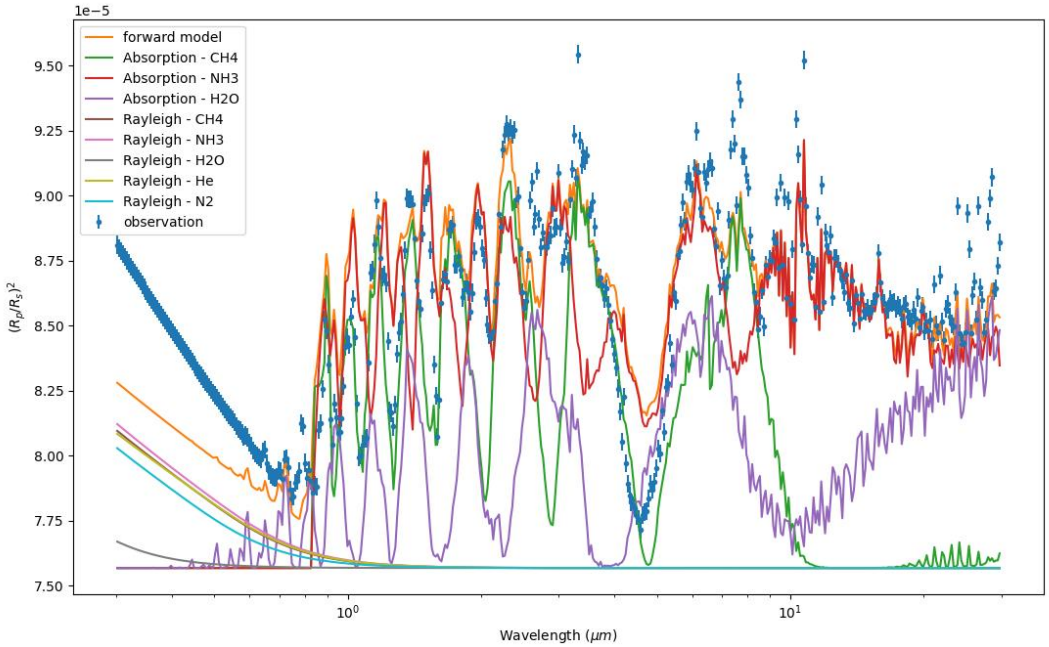

Figure 8b: Plot of the forward model of the Ancient Venus transmission absorption spectrum in TauREx (orange line) against the transmission absorption spectrum simulated in PLATON (blue dots). The axes, individual molecular contributions to the forward model are as for Figure 5c. For this model, the active molecules are CH_4, NH_3 and H_2O. The inactive molecules that contribute to the effects of Rayleigh Scattering are N_2 and He.

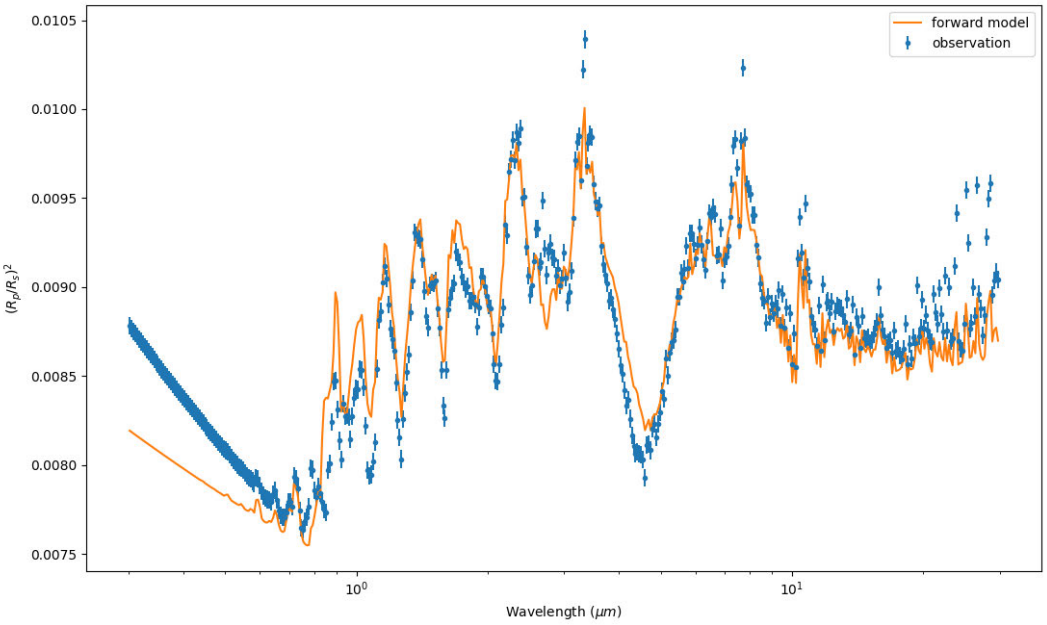

Figure 9a: Plot of the forward model of the TRAPPIST-1b transmission absorption spectrum in TauREx (orange line) against the transmission absorption spectrum simulated in PLATON (blue dots). The x-axis represents the wavelength in microns (µm) as a logarithmic scale, and the y-axis represents the transit depth ($(R_p/R_s)^2$).

The first Venus-like candidate to be modelled was TRAPPIST-1b. Figure 9a displays the simulated transmission absorption spectrum of TRAPPIST-1b from PLATON which was then modelled in TauREx. Similar to the simulated Venus atmosphere, the model of TRAPPIST-1b showed that its atmosphere is also abundant in the active gases CH_4, NH_3 and H_2O. The inactive gases N_2 and He were also present (see Figure 9b). For this model, the strongest absorptions at ~1.3, ~2.2 and ~7.9 µm are caused by CH_4. There is also a small but prominent peak at ~10 µm, which is caused by NH_3. Upon analysis, TRAPPIST-1b is very similar to the simulated Venus models in terms of its atmospheric composition with notable visual similarities between the two transmission absorption spectrums.

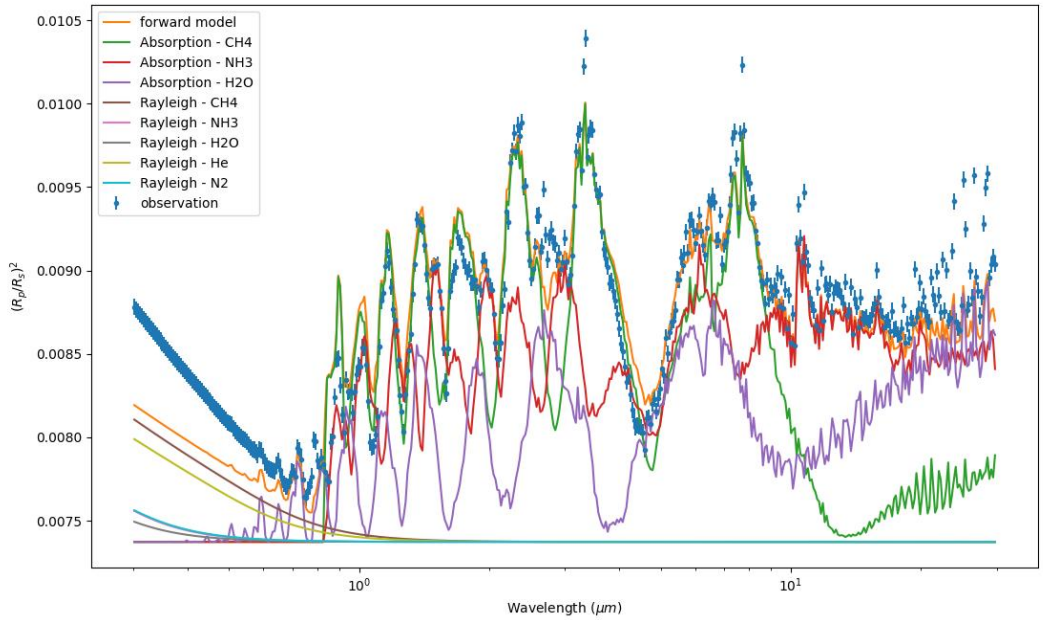

Figure 9b: Plot of the forward model of the TRAPPIST-1b transmission absorption spectrum in TauREx (orange line) against the transmission absorption spectrum simulated in PLATON (blue dots). The x-axis represents the wavelength in microns (µm) as a logarithmic scale, and the y-axis represents the transit depth $((R_p/R_s)^2)$. This plot also contains the individual plots of each molecule's contribution to the planet's modelled transmission absorption spectrum. This includes plots of the individual active and inactive molecules that affect the overall spectral output. For this model, the active molecules are CH_4, NH_3 and H_2O. The inactive molecules that contribute to the effects of Rayleigh Scattering are N_2 and He.

TRAPPIST-1c was the second Venus-like candidate to be modelled (Figure 10a). This exoplanet resides in the same planetary system as TRAPPIST-1b. Visually, the TRAPPIST-1b and TRAPPIST-1c transmission absorption spectrums are very similar. Like Venus and TRAPPIST-1b, TRAPPIST-1c was found to contain the active molecules CH_4, NH_3 and H_2O along with the inactive molecules, N_2 and He. This is shown in Figure 10b. The highest amount of absorption in the TRAPPIST-1c atmosphere occurred at ~1.3, ~2.2 and ~7.9 µm, which is the same absorption pattern as TRAPPIST-1b.

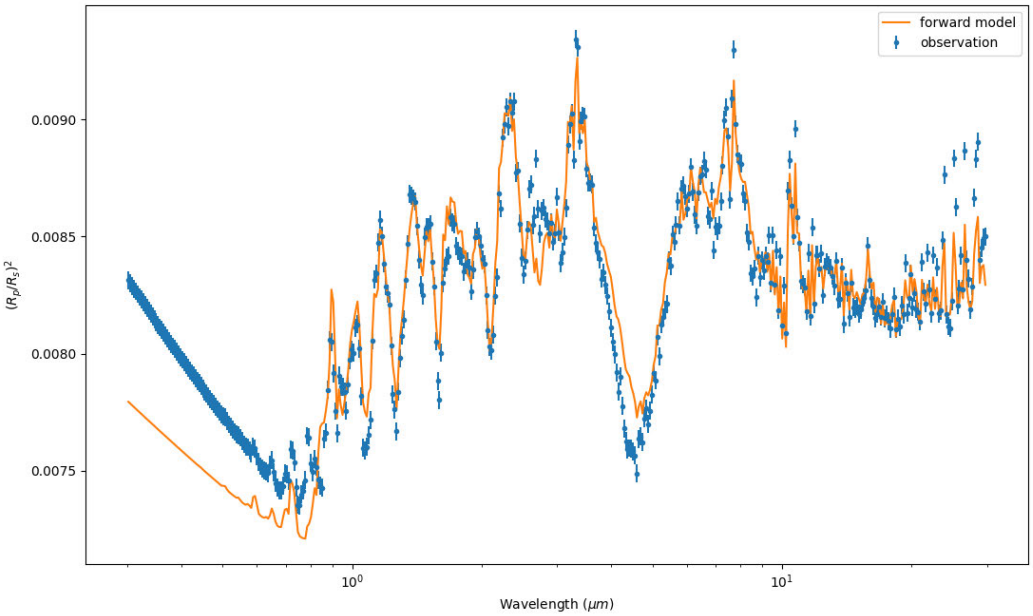

Figure 10a: Plot of the forward model of the TRAPPIST-1c transmission absorption spectrum in TauREx (orange line) against the transmission absorption spectrum simulated in PLATON (blue dots). The x-axis represents the wavelength in microns (µm) as a logarithmic scale, and the y-axis represents the transit depth ($(R_p/R_s)^2$).

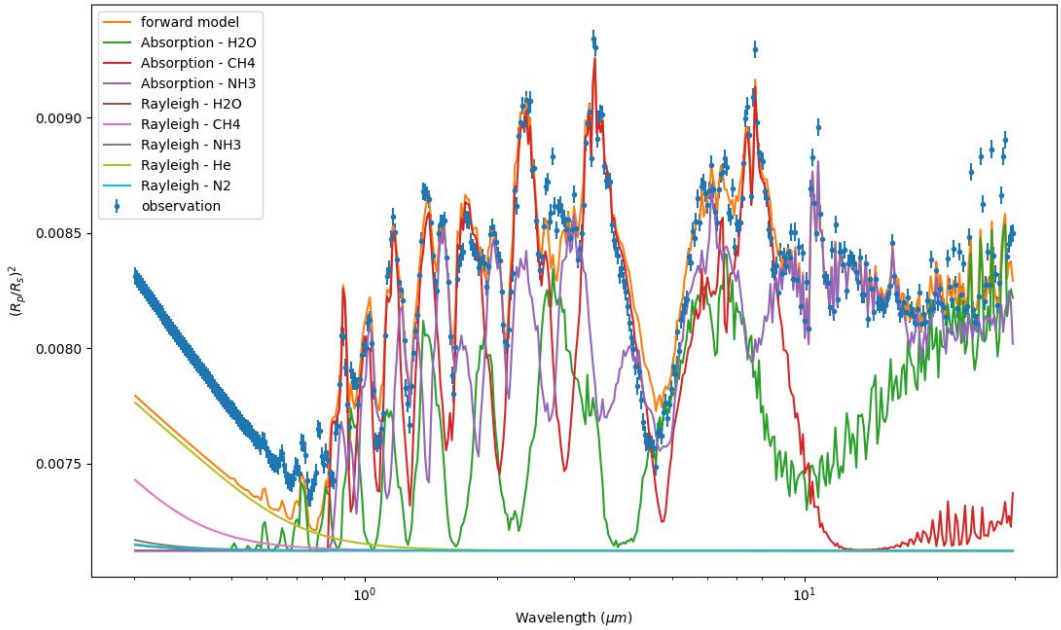

Figure 10b: Plot of the forward model of the TRAPPIST-1c transmission absorption spectrum in TauREx (orange line) against the transmission absorption spectrum simulated in PLATON (blue dots). The axes, individual molecular contributions to the forward model are as for Figure 9b. For this model, the active molecules are CH_4, NH_3 and H_2O. The inactive molecules that contribute to the effects of Rayleigh Scattering are N_2 and He.

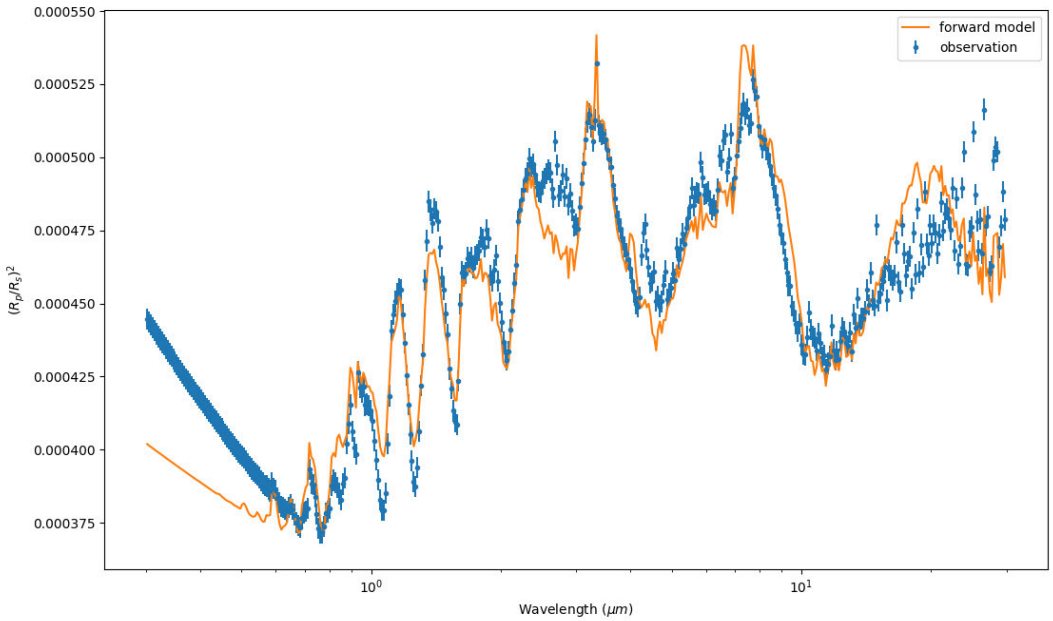

Figure 11a: Plot of the forward model of the GJ 9827c transmission absorption spectrum in TauREx (orange line) against the transmission absorption spectrum simulated in PLATON (blue dots). The x-axis represents the wavelength in microns (µm) as a logarithmic scale, and the y-axis represents the transit depth ($(R_p/R_s)^2$).

GJ 9827c was selected to be modelled due to its distinguished astrophysical parameters. That is, it has a small planet mass and a large planet radius in comparison to Venus. Visually, the atmospheric model of GJ 9827c differs from the simulated Venus model in terms of distinct absorption pattern as seen in Figure 11a. Like TRAPPIST-1b and -1c, the atmosphere of GJ 9827c also contains the active molecules CH_4 and H_2O, as well as the inactive molecules N_2 and He. However, GJ 9827c also shows spectral absorption indicating the presence of SO_2, which has the strongest absorption at ~7.0 and 11.0 μm (Figure 11b). The known Venus atmosphere is the only other model to contain SO_2. Since the PLATON simulations do not account for the effects of volcanic outgassing and runaway greenhouse, SO_2 may be present for other reasons.

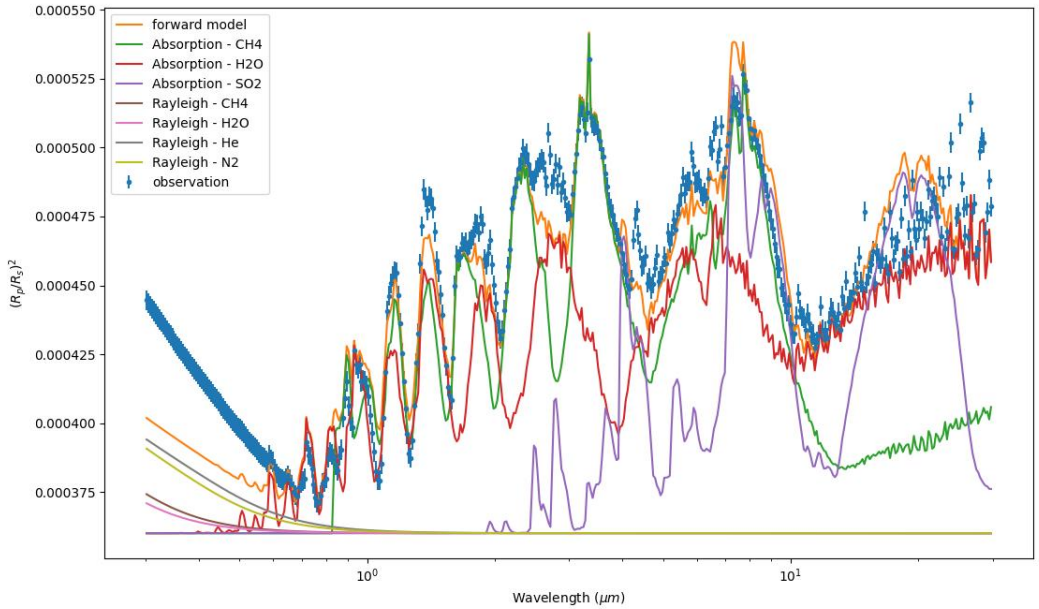

Figure 11b: Plot of the forward model of the GJ 9827c transmission absorption spectrum in TauREx (orange line) against the transmission absorption spectrum simulated in PLATON (blue dots). The x-axis represents the wavelength in microns (µm) as a logarithmic scale, and the y-axis represents the transit depth ($(R_p/R_s)^2$). This plot also contains the individual plots of each molecule's contribution to the planet's modelled transmission absorption spectrum. This includes plots of the individual active and inactive molecules that affect the overall spectral output. For this model, the active molecules are CH_4, SO_2 and H_2O. The inactive molecules that contribute to the effects of Rayleigh Scattering are N_2 and He.

Similar to GJ 9827c, Kepler 138c also has a small planet mass and a large planet radius compared to Venus. However, the model of Kepler 138c's transmission absorption spectrum is more similar to the modelled Venus atmosphere despite the difference in its astrophysical characteristics (Figure 12a). Further analysis of the Kepler 138c model (Figure 12b) determined the presence of active molecules CH_4, NH_3 and H_2O, along with inactive molecules N_2 and He. Like the simulated Venus model, Kepler 138c also has strong absorption at ~1.3, ~2.1 and ~7.6 µm, caused by CH_4. This comparison shows that the planet's astrophysical parameters should not affect the accuracy of the transmission absorption spectral output.

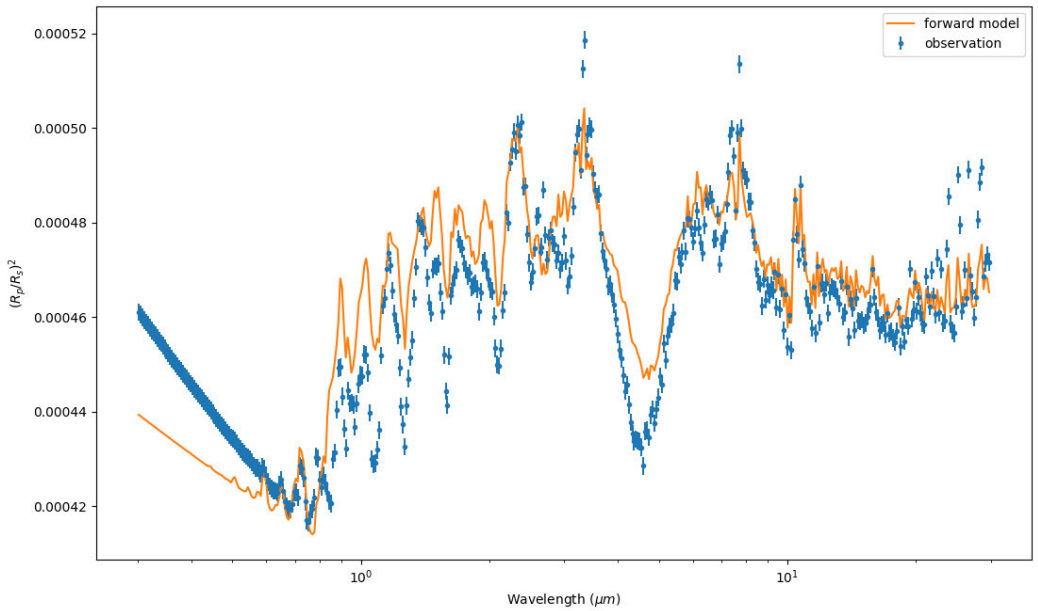

Figure 12a: Plot of the forward model of the Kepler 138c transmission absorption spectrum in TauREx (orange line) against the transmission absorption spectrum simulated in PLATON (blue dots). The x-axis represents the wavelength in microns (µm) as a logarithmic scale, and the y-axis represents the transit depth ($(R_p/R_s)^2$).

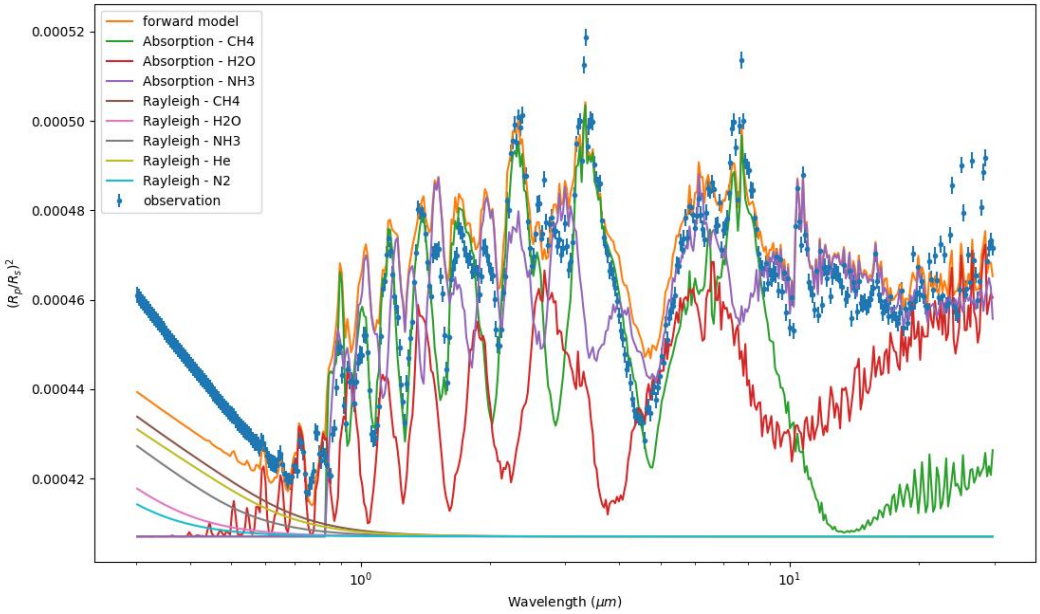

Figure 12b: Plot of the forward model of the Kepler 138c transmission absorption spectrum in TauREx (orange line) against the transmission absorption spectrum simulated in PLATON (blue dots). The axes are as per 7b. This plot also contains the individual plots of each molecule's contribution to the planet's modelled transmission absorption spectrum. This includes plots of the individual active and inactive molecules that affect the overall spectral output. For this model, the active molecules are CH_4, NH_3 and H_2O. The inactive molecules that contribute to the effects of Rayleigh Scattering are N_2 and He.

PLATON calculated the observations shown in the above models by using the astrophysical parameters of the star and planet which includes the star temperature and radius as well as the planet radius, mass, and isothermal temperature. Because of this, PLATON only interprets the information presented by the user and does not make assumptions about the planetary system and its evolutionary status. For example, if the planetary system contains an old, dim star with a small, inner terrestrial planet, it does not assume that the planet has evolved from its ancient status, with a modern and changed atmosphere under its current conditions. Because of this, the PLATON code is limited to only simulating the ancient atmospheric characteristics of an exoplanet given its current astrophysical parameters. This can be seen in Table 9 which presents the fractions of molecular species for each exoplanet in TauREx to fit the observation data simulated in PLATON. Note that these values are relative to the parameters of the exoplanet and are not expected to equal one as shown in section 2.5.2.

By comparing modern Venus to Ancient Venus, where modern Venus uses the known atmospheric molecular abundance and ancient Venus is the simulated Venus model using PLATON, it is apparent that PLATON does not account for factors such as volcanic outgassing and the runaway greenhouse effect. In the modern Venus atmosphere, CO_2, SO_2 and CO are all present whereas the Ancient Venus atmosphere contains CH_4, NH_3 and H_2O. This was also seen with most of the Venus-like candidates, where the molecules present aligned with that of Ancient Venus (see Table 9). The difference in molecules present in the Ancient Venus and Venus-like

candidate atmosphere proves that PLATON does not consider the evolution of the planetary system and how planet atmospheres may change with this.

The simulated and modelled transmission spectral data of the Venus-like candidates can also be compared to real observation data to determine the level of detectability of molecules for different space-based instrumentation. Figure 13 depicts four plots of real transmission spectral data of the TRAPPIST-1 system collected by the HST's WFC3 instrument. Figure 14 depicts JWST simulated transmission spectral data of WASP-79b developed in a program called PandExo plotted with observed data of WASP-79b collected by the HST's WFC3 instrument. From the real observed data, it was determined that strong molecular signals of H_2O, CO and CO_2 could not be detected by the HST WFC3 instrument. In contrast to this, the simulated data from the JWST instruments has the capability to detect these molecules due to its ability to observe in a wider wavelength range and higher resolution.

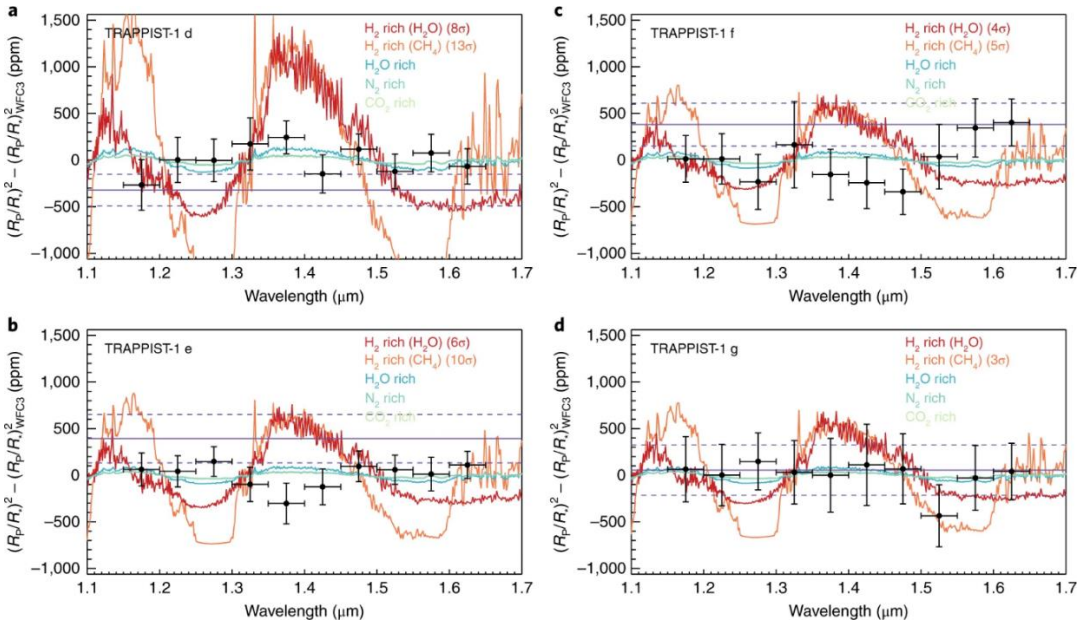

Figure 13: Models of the transmission absorption spectrums of four of the TRAPPIST-1 exoplanetary system using a 3σ uncertainty. Exoplanets in the figure include TRAPPIST-1d, TRAPPIST-1f, TRAPPIST-1e and TRAPPIST-1g. The x-axis represents the wavelength in microns (μm) as a logarithmic scale, and the y-axis represents the calculated transit depth in parts per million (ppm). The observations were developed from four observation points collected by the Hubble Space Telescope's Wide Field Camera 3 (HST WFC3) instrument. The spectra were then analysed using the Markov chain Monte Carlo software and a custom Fortran 90 code. Sourced from (de Wit et al. 2018).

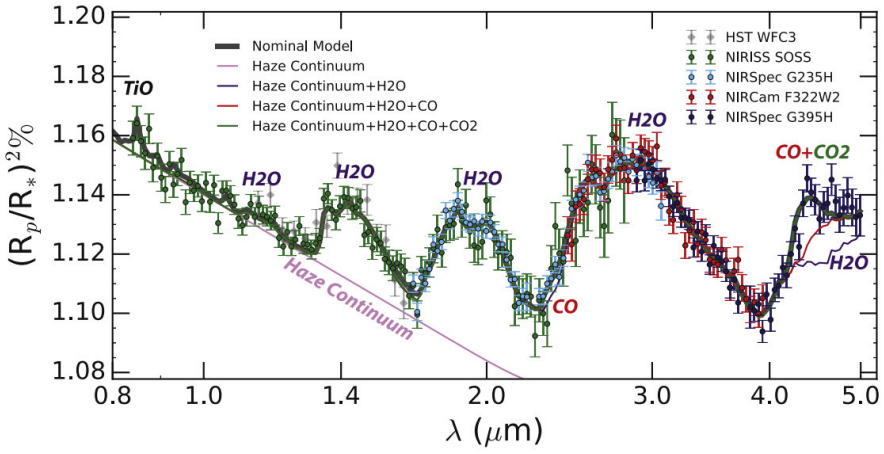

Figure 14: Simulated transmission spectral data of WASP-79b expected to be observed by the JWST instruments (NIRISS, NIRSpec and NIRCam) using the program, PandExo. The simulated data is plotted with the observed transmission spectral data of WASP-79b collected by the HST WFC3 instrument. The plot also depicts the molecules for each transmission peak. These molecules include H_2O, CO and CO_2. Sourced from (Bean, J. et al. 2018).

The above models and existing data presented for comparison provided insight into the classification of exoplanets via atmospheric characterisation. The results will now be discussed in Chapter 6 to further analyse the atmospheric models of the Venus-like candidates.

CHAPTER 6: DISCUSSION

The aim of this project was to characterise the atmospheres of Venus-like candidates to determine the molecular species present in the exoplanet's atmospheres. This would also guide future observations of exoplanets in refining the classification of terrestrial exoplanets.

Venus-like candidates (i.e. exoplanets that have similar astrophysical parameters to Venus) were identified using the NASA Exoplanet Archive. The required parameters for this classification were that the exoplanet must be orbiting a solar analog and have a similar planet radius, mass, and density to Venus. Using this classification scheme, 23 possible Venus-candidates were initially identified.

The astrophysical parameters of the Venus-like candidates were then used in PLATON to model the data for each candidate's transmission absorption spectrums. Of these candidates, only 11 had the parameters required for the PLATON input. Venus and four of the Venus-like candidates were then used for this project. The exoplanets modelled were TRAPPIST-1b, TRAPPIST-1c, GJ 9827c, and Kepler138c (see Section 5.2). These exoplanets were selected to diversify the sample of Venus-like candidates but also include two candidates within the same planetary system for a more complete comparison. PLATON outputted both the plot (see Section 5.1) and the tabulated data of the transmission absorption spectra for each candidate. The outputted tabulated data was then used as the observation input in TauREx.

TauREx was used to characterise the atmospheres of the exoplanets given their astrophysical parameters. In the TauREx models, the temperature profile was set to isothermal, and the pressure profile was set to the default parameters for TauREx for

all models. The abundance identified for each molecular species in the exoplanet atmospheres can be found in Table 9. The atmospheric models for Venus and each of the Venus-like candidates presented in Section 5.2 will be discussed in Section 6.1.

6.1 Interpretation of the Atmospheric Retrievals

6.1.1 Atmospheric Model of Venus

Existing transmission absorption spectral data was available for Venus however, it was not conducive to the TauREx format. Instead, this data was simulated with PLATON using non-runaway greenhouse parameters (i.e. Ancient Venus atmosphere). The atmosphere of this simulation was then modelled using TauREx. Initially, the known abundances of the molecules found in the modern Venus atmosphere were modelled (Figure 7a) and then plotted against the simulated transmission absorption spectrum of Venus from PLATON (Figure 7b). The contribution of active and inactive molecules was also modelled using TauREx (Figure 7c). It is apparent that the simulated spectral data and the modelled spectrum of the known Venus atmosphere do not align. In Figure 7c, the molecules that contribute to the most absorption of light in Venus' atmosphere are CO_2 (green line) and SO_2 (red line). In the TauREx model of the real Venus atmosphere (Figure 7a), most light transmitted through the Venus atmosphere is being absorbed at ~1.8 μm and ~3.4 μm whereas in the PLATON model of Venus' transmission absorption spectrum, light is mostly absorbed at ~2.3 μm and ~10 μm. The difference between the PLATON simulation and TauREx model of the known Venus atmosphere suggests that there are limitations with the PLATON simulations such as its inability to model the effects

of greenhouse gases and volcanic activity on the planetary atmosphere characteristics. This limitation will be considered when comparing the models of Venus and the Venus-like candidates in section 6.1.3.

Another approach was considered to determine the limitations of PLATON and to understand its interpretation of the Venus parameters used for the simulation. Using the Venus spectrum simulated in PLATON, the atmosphere was modelled in TauREx disregarding the known abundances of the molecules in Venus' atmosphere (see Figure 8a). In Figure 8b, we find that the active molecules contributing to the absorption of light are CH_4 (green line), NH_3 (red line), and H_2O (purple line). N_2 (yellow line), which is an inactive molecule, contributes to the effects of Rayleigh Scattering. The abundance of N_2 was increased and decreased to determine if this would change the absorption of light from 0.1 to 0.8 µm, however, there were no significant differences in the outcome. Since there are limitations with the PLATON simulation, the known molecules in Venus' atmosphere cannot be used to determine whether an exoplanet is Venus-like. Instead, the gases found to match the PLATON simulation of Venus were used as a comparison. The gases found to match the PLATON simulation of Venus was more representative of an Ancient Venus atmosphere prior to the volcanic outgassing, which resulted in the runaway greenhouse effect displayed by the modern Venus atmosphere. Considering that PLATON does not account for the effects of greenhouse gases, the resulting atmospheric characteristics were expected.

6.1.2 Atmospheric Models of Venus-like Candidates

6.1.2.1 TRAPPIST-1b

TRAPPIST-1b was the first Venus-like candidate to be modelled in PLATON and TauREx (Figure 9a). Compared to the astrophysical parameters of Venus, TRAPPIST-1b has a similar planet radius of ~0.0969 R_{Jup} but a mass that is approximately one fifth of Venus. TRAPPIST-1b also has a shorter orbital period and a higher isothermal temperature than Venus (see Table 8).

According to the atmospheric model (Figure 9b), the active molecules contributing to the absorption of light in the TRAPPIST-1b are CH_4, NH_3 and H_2O. The inactive molecules that contribute to the effects of Rayleigh Scattering are N_2 and He. The molecules characterised in this atmosphere are identical to those modelled for Venus. According to Table 9, the abundance of CH_4 H_2O in TRAPPIST-1b is relatively higher than ancient Venus but has a lower abundance of NH_3. For TRAPPIST-1b, the highest amount of absorption occurs at ~1.3, ~2.2 and ~7.9 μm. There is also a smaller peak at ~10 μm caused by NH_3 according to Figure 11b, similar to that found in the simulated Venus model (Figure 8a).

Barstow and Irwin (2016) also modelled TRAPPIST-1b atmosphere using the **N**on-linear optimal **E**stimator for **M**ultivariat**E** Spectral Analy**SIS** (NEMESIS), which is a radiative transfer and retrieval code, NEMESIS. Unlike the models presented in this project, Barstow and Irwin (2016) assumed Earth-like characteristics for the TRAPPIST-1b atmosphere. They concluded that TRAPPIST-1b could be a hot present-day Earth, suggesting that it may have an atmosphere similar to ancient Venus. This

model is in alignment with the results found using the PLATON simulations, in this project, of TRAPPIST-1b.

6.1.2.2 TRAPPIST-1c

TRAPPIST-1c was also modelled in TauREx (Figure 10a). TRAPPIST-1c is in the same planetary system as TRAPPIST-1b. TRAPPIST-1c also has similar astrophysical parameters to TRAPPIST-1b. TRAPPIST-1c is further from its star than TRAPPIST-1b (~0.0158 au) and has a lower isothermal temperature of 342 K (see Table 8).

Figure 10b displays the contribution of molecules to the absorption of light in TRAPPIST-1c's atmosphere. According to this model, the active molecules contributing to the absorption of light in the TRAPPIST-1b are H_2O, CH_4 and NH_3. The inactive molecules that contribute to the effects of Rayleigh Scattering are N_2 and He. For TRAPPIST-1c, the highest amount of absorption occurs at ~1.3, ~2.2 and ~7.9 µm, with a small but prominent peak at ~10 µm. Like TRAPPIST-1b, there are also a lot of similarities between the TRAPPIST-1c and simulated Venus models (Figure 8a). According to Table 9, TRAPPIST-1c has a relatively similar molecular abundance to that of TRAPPIST-1b. In terms of the overall spectrum, the intensity of the absorption spectrum is less than TRAPPIST-1b in both peaks and troughs for TRAPPIST-1c. This difference in intensity of the absorption spectrum is caused by the greater orbital distance of TRAPPIST-1c.

According to the parameters in Table 8, TRAPPIST-1b and TRAPPIST-1c are only ~0.02 au apart from each other. Similarities are therefore likely between the atmospheric models of TRAPPIST-1b and TRAPPIST-1c since the astrophysical parameters of the

two exoplanets are similar, and that the PLATON output does not consider other factors such as the effects of runaway greenhouse gases.

Like TRAPPIST-1b, Barstow and Irwin (2016) also modelled TRAPPIST-1c using NEMESIS. This model presented the possibility of TRAPPIST-1c also being a hotter modern Earth, an atmosphere suggested to be similar to ancient Venus. The results of this project, however suggest that its atmosphere would not be of the extent of TRAPPIST-1b.

6.1.2.3 GJ 9827c

According to the parameters in Table 8, GJ 9827c has a smaller planet mass but a larger radius than Venus. It also has a relatively high isothermal temperature of ~811 K. These differences contribute to the diversity of this exoplanet's atmospheric simulation.

The strongest absorption for GJ 9827c occurs at ~2 µm and ~8 µm, where the active molecules that contribute most to the absorption are CH_4, H_2O and SO_2. Again, N_2 and He are inactive molecules contributing to the effects of Rayleigh Scattering (see Figure 11b). Although this model has similar absorption feature to that of the simulated Venus model (Figure 8a), GJ 9827c has an abundance of SO_2 in its atmosphere, a molecule that is found in the modern Venus atmosphere. As seen in Table 9, SO_2 is also relatively low in abundance compared to the other molecules present in the GJ 9827c atmosphere. This is also the same for the abundance of SO_2 in the modern Venus atmosphere. In the modelled contribution of molecules in GJ 9827c's atmosphere (Figure 11b), SO_2 was found to absorb intensely at ~8 µm. This

same peak is found in the model of the modern Venus atmosphere (Figure 7c) which is also caused by SO_2. This means that, unlike modern Venus' atmosphere, the presence of SO_2 in GJ 9827c atmosphere was unlikely the result of outgassing from volcanic activity since the PLATON code does not account for such factors.

Rodriguez et al. (2018) conducted observations of the GJ 9827 system. They found that GJ 9827c is in between a planet that has a radius that can sustain an H/He envelope (gaseous planet) and a planet that has lost its H/He envelope (terrestrial planet), suggesting that this exoplanet may be either a mini-Neptune or a super-Earth. In this project, the model of GJ 9827c infers that it is likely to be a mini-Neptune due to the presence of SO_2 and the age of the planetary system. According to Table 8, the GJ 9827 system had formed ~10 Giga years ago (Gya), which is significantly older than both our solar system (~4.5 Gya) and the TRAPPIST-1 system (>0.5 Gya). The age of the GJ 9827 system suggests that the planets within it, such as GJ 9827c, have experienced events beyond an ancient status. In terms of atmospheric composition, SO_2 is not present in any other terrestrial atmospheric models in this project except for modern Venus. Because PLATON does not consider the effects of volcanic outgassing and runaway greenhouse gases, the presence of SO_2 suggests that GJ 9827c is a gaseous exoplanet.

6.1.2.4 Kepler 138c

Like GJ 9827c, Kepler 138c was modelled due to its diverse astrophysical parameters. As shown in Table 8, Kepler 138c has a larger planet radius but has a smaller planet

mass than Venus. Unlike GJ 9827c, Kepler 138c has a lower isothermal temperature of 398 K, which is more similar to the isothermal temperature of TRAPPIST-1b.

Kepler 138c has a similar transmission absorption spectrum to the simulated Venus model (Figure 8a). From analysis, the Kepler 138c spectral model (Figure 12a) intensely absorbs at ~1.3, ~2.1 and ~7.6 μm, with a notable peak at ~10 μm. Again, these wavelengths resemble the peaks noted from the simulated Venus model (Figure 8a). Upon further analysis of Figure 10b, the active molecules contributing to the absorption in Kepler 138c's atmosphere are CH_4, H_2O and NH_3. The inactive molecules contributing to the effects of Rayleigh Scattering are He and N_2. Again, these are the same molecules that are most abundant in the model of the simulated Venus atmosphere. This model is also similar to the modelled atmospheres of TRAPPIST-1b and TRAPPIST-1c, with varying intensities.

Although Kepler 138c has astrophysical parameters that suggest it may not be terrestrial, projections developed by Almenara et al. (2018) shows that Kepler 138c is likely to have a rocky interior. The thickness of the layer of atmosphere above its interior remains undetermined, which is required to conclude whether this exoplanet is terrestrial or gaseous. Similar to GJ 9827c, this exoplanet is likely within the H/He threshold where it can either contain this type of atmosphere of not. However, the projection of this project suggests that it is terrestrial rather than gaseous due to other factors such as the age of the planetary system and its similar atmospheric composition to ancient Venus.

6.1.3 Comparison of Atmospheric Models of modern and Ancient Venus to Venus-like Candidates

From the TauREx models, it is apparent that TRAPPIST-1b, TRAPPIST-1c and Kepler 138c all exhibit the same atmospheric profile as the simulated Venus model (Figure 8a). That is, they are all similar in terms of their molecular structure as well as the wavelengths of the atmosphere's absorption. However, the transmission absorption spectral models of the Venus-like candidates are only similar to the simulated Venus model and not to the spectral model of Venus with the known atmospheric parameters.

GJ 9827c on the other hand, displayed spectral features that suggest SO_2 is present in its atmosphere. SO_2 is a prominent molecule found in the modern Venus atmosphere, meaning that GJ 9827c may be a modern Venus-like exoplanet. The age of the GJ 9827 system also suggests that GJ 9827c has undergone atmospheric evolution. Because PLATON does not consider the effects of volcanic outgassing and runaway greenhouse gases, it is more likely that GJ 9827c is a gaseous exoplanet.

It has been shown that PLATON can output an accurate transmission absorption spectrum of terrestrial exoplanets in accordance with their parameters. However, PLATON does not account for other factors that may alter the transmission absorption spectrum of exoplanets, such as the effects of runaway greenhouse gases and volcanic activity. This is shown in the model of modern Venus (Figure 7a) using known atmospheric parameters which are abundant in molecules like CO_2 and SO_2, does not match the PLATON spectral output of modern Venus. Unlike the modern Venus model, the simulated Venus model was found to have spectral features of

gases such as CH_4 and NH_3. Because of this marked difference in the known atmosphere of Venus and the simulated model, PLATON does not have the capabilities to account for other atmospheric factors.

Despite PLATON and TauREx being limited by their capability to model certain evolutionary factors, the models are still able to produce extensive detail of a terrestrial atmosphere that has not evolved to extent of modern Venus. This potentially leads to improved spectral simulations of exoplanetary atmospheres and the beginning of an era where we can comprehensively study and understand terrestrial exoplanet atmospheres.

6.1.4 Comparison of Venus-like Candidate Models to Real Instrumentation Capabilities

Since space-based instrumentation is constantly evolving, our current instrumentation's abilities must be considered when searching for Venus-like exoplanets. From Figure 13 and 14, the capabilities of the HST WFC3 instrument and JWST's instruments were analysed using real and simulated transmission spectral observations from de Wit et al. (2018) and Bean et al. (2018). Models of these spectral observations were also developed to identify molecular species. From Figure 13 and 14, it was determined that the HST WFC3 instrument can detect weak signals of H_2O but, is not capable of detecting strong molecular signals of H_2O, CO and CO_2, which are molecules expected to be found in a Venus-like atmosphere. The simulations and models of exoplanets using JWST instruments showed that these same molecules are likely to be detected by JWST. The required percentage transit depth of the Venus-like candidate models can be compared to the JWST capabilities

(see Figure 14). The required percentage transit depth for H_2O at 3µm (in the infrared spectrum) for TRAPPIST-1b and TRAPPIST-1c are ~0.857% and ~0.84%. The differences in the percentage for TRAPPIST-1b and TRAPPIST-1c are due to the distance from their star, where TRAPPIST-1c is further from the star than TRAPPIST-1b. The required percentage transit depth for H_2O at 3 µm for Kepler-138c and GJ 9827c is ~0.005% and ~0.047%, respectively. The percentage of detectability for H_2O appears to correlate with the distance of the exoplanet from the host star. The JWST model of WASP-79b developed by Bean et al. (2018) showed that H_2O at 3µm has a percentage transit depth of 1.15%. Although there is a discrepancy between the models developed for the Venus-like candidates and the JWST model for WASP-79b, they do indicate that the JWST instruments are superior to that of HST. This also means that future spaced-based instrumentation should also exceed the capabilities of JWST. Although not specifically explored here due to the limitations of TauREx, the H_2O comparison given here also gives a good indication of the detectability of other molecules in the infrared spectrum, such as CO_2 and CO.

6.2 Future Directions in Exoplanet Atmospheric Research

In this project, the characterisation of terrestrial exoplanet atmospheres was explored using Venus and Venus-like candidates. Initially, 23 candidates were identified to have astrophysical parameters similar to that of Venus however, only four were modelled in this project. The remaining 19 Venus-like candidates contained a diverse selection of exoplanets that will be considered as candidates in future. The results produced from the four Venus-like candidates indicate that three

of the four exoplanets are likely to have atmospheres similar to that of ancient Venus, which provides insight into the capabilities of current atmospheric modelling programs. Here, the improvements of the modelling programs used in this project will be discussed, as well as the future directions for the characterisation of small, terrestrial exoplanet atmospheres.

6.2.1 Improvements of Modelling using PLATON and TauREx

PLATON and TauREx are predominantly used for modelling gas giant exoplanets. Therefore, the production of spectral outputs for terrestrial exoplanets extends beyond the programs' original capabilities. Their ability to accurately characterise small, terrestrial exoplanets like Earth and Venus, such as the ability to account for the effects of volcanic outgassing, and the effects of runaway greenhouse gases in an atmosphere, is limited. Other geodynamical models, as those modified by Kane et al. (2020), may be used in conjunction with PLATON and TauREx to determine a more accurate transmission absorption spectrum that accounts for other atmospheric factors.

The format of the PLATON data output was not suitable for the TauREx input. This is because PLATON does not calculate the errors associated with the spectral data. For this project, the standard error multiplied by two was used in accordance with Tsiaras et al. (2021), where the errors incapsulated both the cloud and cloud-free simulations. However, a more accurate error would be to calculate the SNR associated with the wavelengths of the spectral output using the JWST Exposure Time Calculator specifically for the JWST instruments.

6.2.2 Future Research of Venus-like Exoplanets

The launch of new space-based observatories and probes such as JWST and the **D**eep **A**tmosphere **V**enus **I**nvestigation of **N**oble gases, **C**hemistry, and **I**maging (DAVINCI) mission will provide promising insight into the unresolved research of atmospheric characterisation with their improved instrumentation.

The JWST is designed to observe in the IR spectrum where previous space telescopes like HST, were limited to the optical and NIR spectrum and, in turn, limited the ability to detect a wider range of molecules in an exoplanet atmosphere. As seen with the model of K2-18b developed by Tsiaras et al. (2021), this also limits the characterisation of an exoplanet's atmosphere. Since JWST is able to observe in a wider spectral range, this will simplify the identification of atmospheric signatures for particular exoplanet atmospheres, such as the atmospheres of Venus-like exoplanets, which will lead to their classification. For the Venus-like candidates used in this project, this may also improve the understanding of the effects of volcanic outgassing and runaway greenhouse gases in small, terrestrial exoplanet atmospheres because of its ability to detect the signatures of CO_2 and SO_2.

DAVINCI is expected to further investigate the atmosphere of Venus, of both its past and present status. In particular, it will be used to understand the effects of volcanic activity which is presumed to have led to modern Venus' extreme atmosphere. Past missions to Venus such as the **Ve**nus **Sp**ectral **R**ocket Experiment (VeSpR) were used to determine the presence of liquid water on ancient Venus. The findings of water escaping in Venus' atmosphere shows that ancient Venus may have had a past atmosphere resembling that of modern Earth.

By combining the research from both missions, a better understanding of Venus' atmospheric evolution will be developed and thus, a better understanding of small, terrestrial exoplanet atmospheres.

CHAPTER 7: CONCLUSION

Currently, there are many confirmed terrestrial candidates residing in planetary systems that have similar astrophysical and geophysical characteristics to terrestrial planets within our solar system, such as Earth and Venus. However, the task of classifying these candidates is challenging due to the limited ability to characterise exoplanet atmospheres with current observation methods and the available space-based instrumentation. With the advancement of technology, such as the recently launched James Webb Space Telescope (JWST), this task may be simplified. Alternative methods can be used to refine the number of terrestrial candidates residing in planetary systems that may exhibit atmospheric characteristics like Earth and Venus. In this project, the characteristics of modern Venus were used to guide the search for terrestrial candidates for atmospheric characterisation. Venus was selected due to its prominent spectral features that are expected to be detected in the optical to IR wavelengths of which JWST can observe (JWST wavelength range = 600 to 28000 nm (ICNIRP 2020)). To guide this alternative method, the following research questions were explored:

1. Can atmospheric simulations of Venus and Venus-like candidates be used to guide the detection of molecular species and key properties of Venus-like exoplanets, using the next generation of space-based observatories?
2. Can these simulations also be used to refine the classification of terrestrial exoplanets, particularly Earth- and Venus-like exoplanets, and assist our understanding of exoplanet and planetary system evolution?

To help answer the above questions, this project provided necessary background information; the details of the methods used; the resulting outcomes from the methods; and a discussion of the contributions of the results to the current understanding and future implications of terrestrial exoplanet atmospheric characterisation.

The literature review (Chapter 2) detailed the current understanding of the Sun, as well as modern Earth, modern Venus, and ancient Venus, to provide a basis for the definition of terrestrial exoplanet atmospheres. The current observational methods and technological limitations were also discussed to emphasise their limitations when detecting and characterising small, terrestrial exoplanets similar to that of Venus and Earth. Specification regarding current and new space-based observatories, such as the Hubble Space Telescope (HST) and JWST in particular, were presented to demonstrate the evolving capabilities of space-based observatories.

Section 2.4 discussed how the parameters of modern Venus was used to guide the search for Venus-like candidates in the NASA Exoplanet Archive database. These parameters included the astrophysical characteristics of Venus and the planetary systems that Venus-like exoplanets may reside in. The astrophysical specifications included the planet mass, radius, and density, as well as the parameters of the host star which included the star temperature and age. These identified parameters were required for the spectral simulations and atmospheric models of Venus and Venus-like candidates using the Python programs, PLATON and TauREx, where an overview

of each program was presented in section 2.5. Finally, section 2.6 gives the context behind the field of research, to provide the direction of this project.

Chapter 3 gives the aims and research questions for this project. The focus of the aims was to emphasise how to overcome the limitations of current methods and instrumentation used to characterise the atmospheres of small terrestrial exoplanets. The aims highlighted the importance of the two research questions stated above.

The methodology (Chapter 4) discussed the parameters of modern Venus used to identify the Venus-like candidates from the NASA Exoplanet Archive which would then be used in the models. The mechanics of the Python programs, PLATON and TauREx, that were used in this project were then detailed. The error calculation used in PLATON was derived from The SciPy community (2022), where the errors were inflated to 2σ to account for the potential cloudy and cloud-free scenarios identified in Tsiaras et al. (2021). This error was incorporated into the PLATON code, which was then outputted with the resulting models in Chapter 5.

Chapter 5 presented the results of this project. The candidate selection from the NASA Exoplanet Archive was systematically narrowed to include Venus, TRAPPIST-1b, TRAPPIST-1c, GJ 9827c and Kepler 138c. TRAPPIST-1b and TRAPPIST-1c were selected since they reside in the same planetary system, whereas GJ 9827c and Kepler 138c were chosen to diversify the candidate sample. The transmission absorption spectrum developed in PLATON for each candidate (including both modern and Ancient Venus) were modelled in TauREx. The input values used for each candidate were listed in Table 8 and 9. Plots of the forward model and simulated

observations were given for each candidate, including the plots of the contributions of the individual molecules to the forward model (Figure 5a to 10b). The results showed that most of the models converged to have similar spectral features to ancient Venus. However, GJ 9827c did not align with the ancient Venus model.

The discussion of the results in Chapter 6 detailed the similarities and differences between the Venus and Venus-like candidate's atmospheres presented in Chapter 5. The absorption features of most of the Venus-like candidates were found to be similar to that of ancient Venus. The main absorption features were noted to be intense at similar wavelengths for TRAPPIST-1b, TRAPPIST-1c and Kepler 138c in comparison to ancient Venus. The contributing molecules for Rayleigh Scattering slightly varied for each output due to the free parameters of TauREx. The molecular species identified in GJ 9827c match the spectral features of modern Venus. PLATON does not consider factors such as volcanic outgassing and runaway greenhouse effect, and considering its astrophysical parameters, this suggests that GJ 9827c is gaseous rather than terrestrial. This was further supported by Rodriguez et al. (2018).

Section 6.2 further discussed the future directions for characterising terrestrial exoplanet atmospheres. This includes increasing the number of exoplanets analysed, improvements to the codes used in this project, and the future direction of space missions to Venus such as DAVINCI.

The outcome of this project provided insight into modelling of atmospheric simulations of small terrestrial exoplanets. The atmospheric models developed in this project showed that there are common molecular species present in the atmospheres of Ancient Venus and the Venus-like candidates. The molecular species

identified are also detectable in the wavelength range of the JWST instruments, meaning that the molecules expected to be in both modern and Ancient Venus-like exoplanets are likely to be detected by the JWST instruments. This claim is supported by Figure 14 which shows that JWST instruments are an improvement compared to past space-based instrumentation, but still requires an increase in capability in order to detect the percentage transit depths required.

The findings in this project and supporting literature show that classification of Earth-like exoplanets are more likely to be Venus-like. This inference can be made from both the astrophysical parameters of the Venus-like candidates and the atmospheric similarities to ancient Venus which are displayed. Not only does this show the misclassification of terrestrial exoplanets, but it also shows the difference between the modern and Ancient Venus atmospheres, which is a result of its evolution. This difference could be used to guide our understanding of planetary evolution and thus, accurately classify terrestrial exoplanets in the future.

The atmospheric simulations and models developed in this project allowed for the identification of the molecular species that are likely present in the Venus-like candidates' atmosphere. Compared to the ancient Venus model and given their astrophysical parameters, most of the Venus-like candidates are likely to be terrestrial. The molecular species identified is potentially detectable in exoplanet atmospheres by instruments that have the capability of observing in the optical to IR wavelengths, such as instruments like JWST and improved future space-based instruments, which will confirm the atmospheric characteristics of exoplanets. This

will lead to the refinement of the classification of confirmed exoplanets to further understand the evolution of planetary systems in future research.

REFERENCES

Agnew, MT, Maddison, ST, Horner, J & Kane, SR 2019, 'Predicting multiple planet stability and habitable zone companions in the TESS era', *Monthly Notices of the Royal Astronomical Society*, vol. 485, no. 4, pp. 4703-25, viewed 24 September 2021, <https://doi.org/10.1093/mnras/stz345>.

Akeson, R, Chen, X, Ciardi, D, Crane, M, Good, J, Harbut, M, Jackson, E, Kane, SR, Laity, A, Leifer, S, Lynn, M, McElroy, D, Papin, M, Plavchan, P, Ramirez, S, Rey, R, Braun, K, Wittman, M, Abajian, M & Zhang, A 2013, 'The NASA Exoplanet Archive: Data and Tools for Exoplanet Research', *Publications of the Astronomical Society of the Pacific*, vol. 125, p. 11, viewed 24 September 2021, <https://iopscience.iop.org/article/10.1086/672273/pdf>.

Al-Refaie, AF, Changeat, Q, Waldmann, IP & Tinetti, G 2021, 'TauREx 3: A Fast, Dynamic, and Extendable Framework for Retrievals', *The Astrophysical Journal*, vol. 917, no. 1, p. 37, viewed 4 April 2022, <https://iopscience.iop.org/article/10.3847/1538-4357/ac0252/meta>.

Almenara, JM, Díaz, RF, Dorn, C, Bonfils, X & Udry, S 2018, 'Absolute densities in exoplanetary systems: photodynamical modelling of Kepler-138', *Monthly Notices of the Royal Astronomical Society*, vol. 478, pp. 460-86, <https://ui.adsabs.harvard.edu/abs/2018MNRAS.478..460A>.

Ando, H, Imamura, T & Tellmann, S 2020, 'Thermal structure of the Venusian atmosphere from the sub-cloud region to the mesosphere as observed by radio occultation', *Scientific Reports*, vol. 10, no. 3448, p. 7, viewed 24 September 2021, <https://doi.org/10.1038/s41598-020-59278-8>.

Barnett, A 2018, *By the Numbers | Sun – NASA Solar System Exploration*, NASA, viewed 23 September 2021, <https://solarsystem.nasa.gov/solar-system/sun/by-the-numbers/>.

Barnett, A 2022, *In Depth | James Webb Space Telescope – NASA Solar System Exploration*, NASA, viewed 30 March 2022, <https://solarsystem.nasa.gov/missions/james-webb-space-telescope/in-depth/>.

Barstow, JK & Irwin, PGJ 2016, 'Habitable worlds with JWST: transit spectroscopy of the TRAPPIST-1 system?', *Monthly Notices of the Royal Astronomical Society*, vol. 461, pp. L92-L6, <https://ui.adsabs.harvard.edu/abs/2016MNRAS.461L..92B>.

Barstow, JK, Aigrain, S, Irwin, PGJ, Kendrew, S & Fletcher, LN 2015, 'Transit spectroscopy with James Webb Space Telescope: systematics, starspots and stitching', *Monthly Notices of the Royal Astronomical Society*, vol. 448, no. 3, pp. 2546-61, <https://academic.oup.com/mnras/article/448/3/2546/1109920>.

Barstow, JK, Changeat, Q, Garland, R, Line, MR, Rocchetto, M & Waldmann, IP 2020, 'A comparison of exoplanet spectroscopic retrieval tools', *Monthly Notices of the Royal Astronomical Society*, vol. 493, no. 4, pp. 4884-909, viewed 24 September 2021, <https://doi.org/10.1093/mnras/staa548>.

Basilevsky, AT & Head, JW 2003, 'The surface of Venus', *Reports on Progress in Physics*, vol. 66, no. 1699, <https://iopscience.iop.org/article/10.1088/0034-4885/66/10/R04>.

Bean, J, Stevenson, K, Batalha, N, Berta-Thompson, Z, Kreidberg, L, Crouzet, N, Benneke, B, Line, MR, Sing, DK & Wakeford, HR 2018, 'The Transiting Exoplanet Community Early Release Science Program for JWST', *Publications of the Astronomical Society of the Pacific*, vol. 130, no. 993, p. 114402, <https://iopscience.iop.org/article/10.1088/1538-3873/aadbf3>.

Bean, J, Stevenson, K, Batalha, N, Berta-Thompson, Z, Kreidberg, L, Crouzet, N, Benneke, B, Line, M, Sing, D, Wakeford, H, Knutson, H, Kempton, E, Désert, J, Crossfield, I, Batalha, N, de Wit, J, Parmentier, V, Harrington, J, Moses, J, Lopez-Morales, M, Alam, M, Blecic, J, Bruno, G, Carter, A, Chapman, J, Decin, L, Dragomir, D, Evans, T, Fortney, J, Fraine, J, Gao, P, García Muñoz, A, Gibson, N, Goyal, J, Heng, K, Hu, R, Kendrew, S, Kilpatrick, B, Krick, J, Lagage, P, Lendl, M, Louden, T, Madhusudhan, N, Mandell, A, Mansfield, M, May, E, Morello, G, Morley, C, Nikolov,

N, Redfield, S, Roberts, J, Schlawin, E, Spake, J, Todorov, K, Tsiaras, A, Venot, O, Waalkes, W, Wheatley, P, Zellem, R, Angerhausen, D, Barrado, D, Carone, L, Casewell, S, Cubillos, P, Damiano, M, de Val-Borro, M, Drummond, B, Edwards, B, Endl, M, Espinoza, N, France, K, Gizis, J, Greene, T, Henning, T, Hong, Y, Ingalls, J, Iro, N, Irwin, P, Kataria, T, Lahuis, F, Leconte, J, Lillo-Box, J, Lines, S, Lothringer, J, Mancini, L, Marchis, F, Mayne, N, Palle, E, Rauscher, E, Roudier, G, Shkolnik, E, Southworth, J, Swain, M, Taylor, J, Teske, J, Tinetti, G, Tremblin, P, Tucker, G, van Boekel, R, Waldmann, I, Weaver, I & Zingales, T 2018, 'The Transiting Exoplanet Community Early Release Science Program for JWST', *Publications of the Astronomical Society of the Pacific*, vol. 130, p. 114402, <https://ui.adsabs.harvard.edu/abs/2018PASP..130k4402B>.

Belleville, M 2021, *Observatory | NASA*, NASA, viewed 30 March 2022, <https://www.nasa.gov/mission_pages/hubble/observatory>.

Brennen, P 2021, *Transiting Exoplanet Survey Satellite (TESS)*, NASA, viewed 30 March 2022, <https://exoplanets.nasa.gov/tess/>.

California Institute of Technology 2019, *Solar System Sizes and Distances*, Jet Propulsion Laboratory, viewed 16 September 2021, <https://www.jpl.nasa.gov/edu/pdfs/scaless_reference.pdf>.

Caltech 2021, *NASA Exoplanet Archive*, NASA, viewed 25 August 2021, <https://exoplanetarchive.ipac.caltech.edu/ >.

Caltech 2022, *The Multiple Instrument Chamber - NASA Spitzer Space Telescope*, Caltech, viewed 30 March 2022, <http://legacy.spitzer.caltech.edu/mission/182-The-Multiple-Instrument-Chamber#:~:text=Spitzer's%20Multiple%20Instrument%20Chamber%20contains,Spectrograph%20and%20Multiband%20Imaging%20Photometer>.

Chance, KV & Spurr, RJD 1997, 'Ring effect studies: Rayleigh scattering, including molecular parameters for rotational Raman scattering, and the Fraunhofer

spectrum', *Applied Optics*, vol. 36, no. 21, pp. 5224-3230, <https://lweb.cfa.harvard.edu/atmosphere/publications/1997AOring.pdf>.

Charnay, B, Wolf, ET, Marty, B & Forget, F 2020, 'Is the Faint Young Sun Problem for Earth Solved?', *Space Science Reviews*, vol. 216, no. 5, viewed 24 September 2021, <https://doi.org/10.1007/s11214-020-00711-9>.

Climate Policy Watcher 2022, *Scattering by molecules Rayleigh Scattering*, Climate Policy Watcher, viewed 30 May 2022, <https://www.climate-policy-watcher.org/surface-temperature/scattering-by-molecules-rayleigh-scattering.html>.

CSIRO 2021, *Luminosity of Stars*, CSIRO Astronomy and Space Science, viewed 20 August 2021, <https://www.atnf.csiro.au/outreach/education/senior/astrophysics/photometry_luminosity.html>.

de Wit, J, Wakeford, H, Lewis, N, Delrez, L, Gillon, M, Selsis, F, Leconte, J, Demory, B, Bolmont, E, Bourrier, V, Burgasser, A, Grimm, S, Jehin, E, Lederer, S, Owen, J, Stamenković, V & Triaud, A 2018, 'Atmospheric reconnaissance of the habitable-zone Earth-sized planets orbiting TRAPPIST-1', *Nature Astronomy*, vol. 2, pp. 214-9, <https://ui.adsabs.harvard.edu/abs/2018NatAs...2..214D>.

Deeg, H & Alonso, R 2018, 'Transit Photometry as an Exoplanet Discovery Method', in HJ Deeg & JA Belmonte (eds), *Handbook of Exoplanets*, Springer International Publishing, Cham, pp. 633-57, viewed 29 September 2021, <https://doi.org/10.1007/978-3-319-55333-7_117>.

Encrenaz, T 2014, 'Infrared spectroscopy of exoplanets: observational constraints', *The Royal Society Publishings*, vol. 372, no. 2014, viewed 30 March 2022, <https://ui.adsabs.harvard.edu/abs/2022Icar..37614885E>.

ESA 2022a, *Hubble's Instruments: COS - Cosmic Origins Spectrograph | ESA/Hubble | ESA/Hubble*, European Space Agency (ESA), viewed 30 March 2022, <https://esahubble.org/about/general/instruments/cos/>.

ESA 2022b, *Hubble's Instruments: WFC3 - Wide Field Camera 3 | ESA/Hubble | ESA/Hubble*, European Space Agency (ESA), viewed 30 March 2022, <https://esahubble.org/about/general/instruments/wfc3/>.

ESA 2022c, *Hubble's instruments: ACS - Advanced Camera for Surveys | ESA/Hubble | ESA/Hubble*, European Space Agency (ESA), viewed 30 March 2022, <https://esahubble.org/about/general/instruments/acs/>.

Garner, R 2017a, *Hubble Space Telescope – Wide Field Camera 3 | NASA*, NASA, viewed 30 March 2022, <https://www.nasa.gov/content/hubble-space-telescope-wide-field-camera-3>.

Garner, R 2017b, *Hubble Space Telescope – Advanced Camera for Surveys | NASA*, NASA, viewed 30 March 2022, <https://www.nasa.gov/content/hubble-space-telescope-advanced-camera-for-surveys>.

Garner, R 2019, *Hubble Space Telescope - Space Telescope Imaging Spectrograph | NASA*, NASA, viewed 30 March 2022, <https://www.nasa.gov/content/hubble-space-telescope-space-telescope-imaging-spectrograph>.

Garner, R 2020, *TESS - Transiting Exoplanet Survey Satellite | NASA*, NASA, viewed 30 March 2022, <https://www.nasa.gov/tess-transiting-exoplanet-survey-satellite>.

Gillon, M, Jehin, E, Lederer, S, Delrez, L, de Wit, J, Burdanov, A, Grootel, V, Burgasser, A, Triaud, A, Opitom, C, Demory, B, Sahu, D, Gagliuffi, D, Magain, P & Queloz, D 2016, 'Temperate Earth-sized planets transiting a nearby ultracool dwarf star', *Nature*, vol. 533, pp. 221-4.

Gordon, IE, Rothman, LS, Hargreaves, RJ, Hashemi, R, Karlovets, EV, Skinner, FM, Conway, EK, Hill, C, Kochanov, RV, Tan, Y, Wcisło, P, Finenko, AA, Nelson, K, Bernath, PF, Birk, M, Boudon, V, Campargue, A, Chance, KV, Coustenis, A, Drouin, BJ, Flaud, J-M, Gamache, RR, Hodges, JT, Jacquemart, D, Mlawer, EJ, Nikitin, AV, Perevalov, VI, Rotger, M, Tennyson, J, Toon, GC, Tran, H, Tyuterev, VG, Adkins, EM,

Baker, A, Barbe, A, Canè, E, Császár, AG, Dudaryonok, A, Egorov, O, Fleisher, AJ, Fleurbaey, H, Foltynowicz, A, Furtenbacher, T, Harrison, JJ, Hartmann, J-M, Horneman, V-M, Huang, X, Karman, T, Karns, J, Kassi, S, Kleiner, I, Kofman, V, Kwabia-Tchana, F, Lavrentieva, NN, Lee, TJ, Long, DA, Lukashevskaya, AA, Lyulin, OM, Makhnev, VY, Matt, W, Massie, ST, Melosso, M, Mikhailenko, SN, Mondelain, D, Müller, HSP, Naumenko, OV, Perrin, A, Polyansky, OL, Raddaoui, E, Raston, PL, Reed, ZD, Rey, M, Richard, C, Tóbiás, R, Sadiek, I, Schwenke, DW, Starikova, E, Sung, K, Tamassia, F, Tashkun, SA, Vander Auwera, J, Vasilenko, IA, Vigasin, AA, Villanueva, GL, Vispoel, B, Wagner, G, Yachmenev, A & Yurchenko, SN 2022, 'The HITRAN2020 molecular spectroscopic database', *Journal of Quantitative Spectroscopy and Radiative Transfer*, vol. 277, p. 107949, <https://ui.adsabs.harvard.edu/abs/2022JQSRT.27707949G>.

Hall, S 2019, 'Venus is Earth's evil twin — and space agencies can no longer resist its pull', *Nature*, vol. 570, pp. 20-5, viewed 24 September 2021, <https://doi.org/10.1038/d41586-019-01730-5>.

Hansen, JE & Travis, LD 1974, 'Light scattering in planetary atmospheres', *Space Science Reviews*, vol. 16, pp. 527-610, <https://articles.adsabs.harvard.edu/full/1974SSRv...16..527H/0000555.000.html>.

Hoeijmakers, HJ, Snellen, IAG & van Terwisga, SE 2018, 'Searching for reflected light from τ Bootis b with high-resolution ground-based spectroscopy: Approaching the 10−5 contrast barrier', *Astronomy & Astrophysics*, vol. 610, p. 14, viewed 30 March 2022, < https://ui.adsabs.harvard.edu/abs/2018A&A...610A..47H>.

ICNIRP 2020, *ICNIRP | Infrared (780 nm-1mm)*, International Commission for Non-Ionizing Radiation Protection, viewed 30 March 2022, <https://www.icnirp.org/en/frequencies/infrared/index.html>.

Johnson, M 2017, *Spacecraft and Instrument | NASA*, NASA, viewed 30 March 2022, <https://www.nasa.gov/mission_pages/kepler/spacecraft/index.html>.

Kane, SR, Kopparapu, RK & Domagal-Goldman, S 2014, 'On the Frequency of Potential Venus Analogs from Kepler Data', *The Astrophysical Journal Letters*, vol.

794, no. 1, viewed 24 September 2021, <https://doi.org/10.1088/2041-8205/794/1/L5>.

Kane, SR, Ceja, AY, Way, MJ & Quintana, EV 2018, 'Climate Modeling of a Potential ExoVenus', *The Astrophysical Journal*, vol. 869, no. 1, p. 9, viewed 24 September 2021, <https://iopscience.iop.org/article/10.3847/1538-4357/aaec68/pdf>.

Kane, SR, Roettenbacher, RM, Unterborn, CT, Foley, BJ & Hill, ML 2020, 'A Volatile-poor Formation of LHS 3844b Based on Its Lack of Significant Atmosphere', *The Planetary Science Journal*, vol. 1, p. 36, <https://ui.adsabs.harvard.edu/abs/2020PSJ.....1...36K>.

Kane, SR, Arney, G, Crisp, D, Domagal-Goldman, S, Glaze, LS, Goldblatt, C, Grinspoon, D, Head, JW, Lenardic, A, Unterborn, C, Way, MJ & Zahnle, KJ 2019, 'Venus as a laboratory for exoplanetary science', *Journal of Geophysical Research: Planets*, vol. 124, pp. 2015-28, viewed 24 September 2021, <https://doi.org/10.1029/2019JE005939>.

Kasting, JF & Siefert, JL 2002, 'Life and the Evolution of Earth's Atmosphere', *Science*, vol. 296, no. 5570, viewed 24 September 2021, <https://www.science.org/doi/full/10.1126/science.107118>.

Kopparapu, RK, Ramirez, R, Kasting, JF, Eymet, V, Robinson, TD, Mahadevan, S, Terrien, RC, Domagal-Goldman, S, Meadows, V & Deshpande, R 2013, 'Habitable Zones around Main-Sequence Stars: New Estimates', *The Astrophysical Journal*, vol. 765, no. 2, p. 16pp, viewed 24 September 2021, <http://dx.doi.org/10.1088/0004-637X/765/2/131>.

Kreidberg, L, Bean, JL, Desert, J, Benneke, B, Deming, D, Stevenson, K, Seager, S, Berta-Thompson, Z, Seifahrt, A & Homeier, D 2014, 'Clouds in the atmosphere of the super-Earth exoplanet GJ 1214b', *Nature*, vol. 505, pp. 69-72, <https://www.nature.com/articles/nature12888#citeas>.

Lammer, H, Zerkle, AL, Gebauer, S, Tosi, N, Noack, L, Scherf, M, Pilat-Lohinger, E, Gudel, M, Grenfell, JL, Godolt, M & Nikolaou, A 2018, 'Origin and evolution of the atmospheres of early Venus, Earth and Mars', *The Astronomy and Astrophysics*

Review, vol. 26, no. 2, p. 72, viewed 24 September 2021, <https://doi.org/10.1007/s00159-018-0108-y>.

Ligman, M 2021, 'A brief history of the term 'habitable zone' in the 19th century', *International Journal of Astrobiology*, pp. 1-5, viewed 24 September 2021, <https://doi.org/10.1017/S1473550421000203>.

Luginin, M, Fedorova, A, Belyaev, D, Montmessin, F, Wilquet, V, Korablev, O, Bertaux, JL & Vandaele, AC 2016, 'Aerosol properties in the upper haze of Venus from SPICAV IR data', *Icarus*, vol. 277, pp. 154-70, viewed 24 September 2021, <https://doi.org/10.1016/j.icarus.2016.05.008>.

Markiewicz, W, Titov, D, Limaye, S, Keller, HU, Ignatiev, N, Jaumann, R, Thomas, N, Michalik, H, Moissl, R & Russo, P 2007, 'Morphology and dynamics of the upper cloud layer of Venus', *Nature*, vol. 450, pp. 633-6, viewed 24 September 2021, <https://doi.org/10.1038/nature06320>.

McGregor, V, Jackson, R, Greicius, T & Hartono, N 2022, *Universe Missions - NASA Jet Propulsion Laboratory*, viewed 30 March 2022, <https://www.jpl.nasa.gov/missions/spitzer-space-telescope>.

Mighell, K & van Cleve, J 2020, *K2*, NASA, viewed 30 March 2022, <https://archive.stsci.edu/files/live/sites/mast/files/home/missions-and-data/k2/_documents/KSCI-19116-003.pdf>.

MIT 2022, *TESS - Transiting Exoplanet Survey Satellite*, Massachussetts Institute of Technology (MIT), viewed 30 March 2022, <https://tess.mit.edu/>.

NASA 2017, *Planet Detection Methods | NASA*, NASA, viewed 23 June 2021, <<https://www.nasa.gov/kepler/overview/planetdetectionmethods>>.

NASA 2020, *Comparison: Webb vs Hubble Telescope - Webb/NASA*, NASA, viewed 30 March 2022, <https://www.jwst.nasa.gov/content/about/comparisonWebbVsHubble.html#wavelength>.

NASA 2021, *Terrestrial | Planet Types – Exoplanet Exploration: Planets Beyond our Solar System*, NASA, viewed 30 July 2021, <https://exoplanets.nasa.gov/what-is-an-exoplanet/planet-types/terrestrial/>.

NASA 2022a, *Fine Guidance Sensor/Near InfraRed Imager and Slitless Spectrograph (FGS/NIRISS) Webb/NASA*, NASA, viewed 30 March 2022, <https://jwst.nasa.gov/content/observatory/instruments/fgs.html>.

NASA 2022b, *Exoplanets*, NASA, viewed 30 March 2022, <https://www.spitzer.caltech.edu/mission/exoplanets>.

NASA Ames 2021, *Light Curve of a Planet Transiting Its Star – Exoplanet Exploration: Planets Beyond our Solar System*, NASA Ames,, viewed 4 April 2022, <https://exoplanets.nasa.gov/resources/280/light-curve-of-a-planet-transiting-its-star/>.

NASA Exoplanet Science Institute 2021a, *NASA Exoplanet Archive*, 29 September 2021, <https://exoplanetarchive.ipac.caltech.edu/cgi-bin/TblView/nph-tblView?app=ExoTbls&config=PS>.

NASA Exoplanet Science Institute 2021b, *NASA Exoplanet Archive Overview and Holdings*, NASA, viewed 24 September 2021, <https://exoplanetarchive.ipac.caltech.edu/docs/intro.html>.

Niraula, P, Redfield, S, Dai, F, Barragán, O, Gandolfi, D, Cauley, PW, Hirano, T, Korth, J, Alexis, M, Smith, S, Prieto-Arranz, J, Grziwa, S, Fridlund, M, Persson, CM, Justesen, AB, Winn, JN, Albrecht, S, Cochran, WD, Csizmadia, S, Duvvuri, GM, Endl, M, Hatzes, AP, Livingston, JH, Narita, N, Nespral, D, Nowak, G, Pätzold, M, Palle, E & Van Eylen, V 2018, 'Three Super-Earths Transiting the nearby star GJ 9827', vol. 231, p. 104.05, <https://ui.adsabs.harvard.edu/abs/2018AAS...23110405N>.

Planetary Sciences Inc. 2019, *Stable Habitable Zone*, Planetary Science Inc., viewed 23 September 2021, <https://planetary-science.org/astrobiology/stable-habitable-zone/>.

Pontoppidan, KM, Pickering, TE, Laidler, VG, Gilbert, K, Sontag, CD, Slocum, C, Sienkiewicz, MJ, Hanley, C, Earl, NM, Pueyo, L, Ravindranath, S, Karakla, DM, Robberto, M, Noriega-Crespo, A & Barker, EA 2016, 'Pandeia: a multi-mission exposure time calculator for JWST and WFIRST', *Observatory Operations: Strategies, Processes, and Systems VI*, p. 991016, <https://ui.adsabs.harvard.edu/abs/2016SPIE.9910E..16P>.

Pyle, T 2020, *Kepler/K2 | Center for Astrophysics*, Center for Astrophysics: Harvard & Smithsonian, viewed 30 March 2022, <https://pweb.cfa.harvard.edu/facilities-technology/telescopes-instruments/keplerk2>.

Pyle, T 2021, *Transiting Exoplanet Survey Satellite (TESS) | Center for Astrophysics*, Center for Astrophysics: Harvard & Smithsonian, viewed 30 March 2022, <https://pweb.cfa.harvard.edu/facilities-technology/telescopes-instruments/transiting-exoplanet-survey-satellite-tess>.

Quanz, SP, Absil, O, Benz, W, Bonfils, X, Berger, JP, Defrere, D, van Dishoeck, E, Ehrenreich, D, Fortney, J & Glauser, A 2021, 'Atmospheric characterization of terrestrial exoplanets in the mid-infrared: biosignatures, habitability, and diversity', *Experimental Astronomy*, viewed 30 March 2022, <https://ui.adsabs.harvard.edu/abs/2021ExA...tmp..118Q>.

Reike, GH, Wright, GS, Boker, T, Bouwman, J, Colina, L, Glasse, A, Gordon, KD, Greene, TP, Gudel, M & Henning, T 2015, 'The Mid-Infrared Instrument for the James Webb Space Telescope, I: Introduction', *Publications of the Astronomical Society of the Pacific*, vol. 127, no. 953, p. 584, viewed 30 March 2022, <https://iopscience.iop.org/article/10.1086/682252>.

Robinson, TD, Fortney, JJ & Hubbard, WB 2017, 'Analytic Scattering and Refraction Models for Exoplanet Transit Spectra', *The Astrophysical Journal*, vol. 850, no. 2, p. 128, <https://iopscience.iop.org/article/10.3847/1538-4357/aa951e/meta>.

Rodriguez, JE, Vanderburg, A, Eastman, JD, Mann, AW, Crossfield, IJM, Ciardi, DR, Latham, DW & Quinn, SN 2018, 'A System of Three Super Earths Transiting the Late K-Dwarf GJ 9827 at 30 pc', *The Astronomical Journal*, vol. 155, p. 72, <https://ui.adsabs.harvard.edu/abs/2018AJ....155...72R>.

Santos, WC & Amorium, RGG 2017, 'Transit method and discovery of exoplanet', *Revista Brasileira de Ensino de Fisica*, vol. 39, no. 2, p. 8, viewed 24 September 2021, <https://www.scielo.br/j/rbef/a/gCsTTSM8XypVnqVpyj8xJqJ/?lang=pt>.

Sing, DK, Lecavelier des Etangs, A, Fortney, JJ, Burrows, AS, Pont, F, Wakeford, HR, Ballester, GE, Nikolov, N, Henry, GW, Aigrain, S, Deming, D, Evans, TM, Gibson, NP, Huitson, CM, Knutson, H, Showman, AP, Vidal-Madjar, A, Wilson, PA, Williamson, MH & Zahnle, K 2013, 'HST hot-Jupiter transmission spectral survey: evidence for aerosols and lack of TiO in the atmosphere of WASP-12b', *Monthly Notices of the Royal Astronomical Society*, vol. 436, no. 4, pp. 2956-73, viewed 30 March 2022, <https://ui.adsabs.harvard.edu/abs/2013MNRAS.436.2956S>.

Soderblom, DR & King, JR 1997, 'Solar-Type Stars: Basic Information on Their Classification and Characterization', *The Second Annual Lowell Observatory Fall Workshop*, Space Telescope Science Institute, Baltimore MD, viewed 24 September 2021, <http://www2.lowell.edu/users/jch/workshop/drs/drs-p1.html>.

Space Telescope Science Institute 2020, *Instrumentation*, Space Telescope Science Institute, viewed 30 March 2022, <https://www.stsci.edu/jwst/instrumentation>.

Space Telescope Science Institute 2021, *Mikulski Archive for Space Telescopes: About MAST*, MAST, viewed 23 September 2021, <https://archive.stsci.edu/>.

Space Telescope Science Institute 2022a, *Hubble Space Telescope: Observer's Guide Winter 2022*, Space Telescope Science Institute, viewed 30 March 2022,

<https://www.stsci.edu/files/live/sites/www/files/home/hst/_documents/HST-Booklet.pdf>.

Space Telescope Science Institute 2022b, *MIRI Imaging - JWST User Documentation*, Space Telescope Science Institute, viewed 30 March 2022, <https://jwst-docs.stsci.edu/jwst-mid-infrared-instrument/miri-observing-modes/miri-imaging>.

Space Telescope Science Institute 2022c, *JWST Near Infrared Imager and Slitless Spectrograph - JWST User Documentation*, Space Telescope Science Institute, viewed 30 March 2022, <https://jwst-docs.stsci.edu/jwst-near-infrared-imager-and-slitless-spectrograph>.

Swinburne University of Technology 1999, *Harvard Spectral Classification | COSMOS*, Swinburne University of Technology, COSMOS, viewed 20 August 2021, <https://astronomy.swin.edu.au/cosmos/h/harvard+spectral+classification>.

Tasker, E, Tan, J & Heng, K 2017, 'The language of exoplanet ranking metrics needs to change', *Nature Astronomy*, vol. 1, viewed 23 September 2021, <https://doi.org/10.1038/s41550-017-0042>.

Taylor, FW, Svedhem, H & Head III, JW 2018, 'Venus: The Atmosphere, Climate, Surface, Interior and Near-Space Environment of an Earth-Like Planet', *Space Science Reviews*, vol. 214, no. 35, viewed 23 September 2021, <https://doi.org/10.1007/s11214-018-0467-8>.

The SciPy community 2022, *scipy.stats.sem — SciPy v1.8.1 Manual*, viewed 3 June 2022, <https://docs.scipy.org/doc/scipy/reference/generated/scipy.stats.sem.html>.

Titov, DV, Ignatiev, NI, McGouldrick, K, Wilquet, V & Wilson, CF 2018, 'Clouds and Hazes of Venus', *Space Science Reviews*, vol. 43, no. 16, p. 61, viewed 23 September 2021, <https://doi.org/10.1007/s11214-018-0552-z>.

Tsiaras, A, Waldmann, IP, Tinetti, G, Tennyson, J & Yurchenko, SN 2021, 'Water vapour in the atmosphere of the habitablezone eight-Earth-mass planet K2-18 b', *Nature Astronomy*, vol. 3, pp. 1086-91, <https://www-nature-com.ezproxy.usq.edu.au/articles/s41550-019-0878-9.pdf>.

Udry, S & Santos, NC 2007, 'Statistical Properties of Exoplanets', *Annual Review of Astronomy and Astrophysics*, vol. 45, pp. 397-439, viewed 23 September 2021, <https://doi.org/10.1146/annurev.astro.45.051806.110529>.

University of Arizona 2016, *Space versus Ground Telescopes*, University of Arizona, viewed 30 March 2022, <https://research.arizona.edu/stories/space-versus-ground-telescopes>.

Uppsala University 2022, *Exoplanet atmospheres - Department of Physics and Astronomy - Uppsala University, Sweden*, Uppsala University, viewed 3 April 2022, <https://www.physics.uu.se/research/astronomy-and-space-physics/research/planets/exoplanet-atmospheres/>.

Vanderspek, R, Doty, JP, Fausnaugh, M, Villasenor, JNS, Jenkins, JM, Burke, CJ & Ricker, GR 2018, *TESS Instrument Handbook*, NASA, viewed 30 March 2022, <https://archive.stsci.edu/missions/tess/doc/TESS_Instrument_Handbook_v0.1.pdf>.

Voytek, MA 2009, *Kepler | Missions | Astrobiology*, NASA, viewed 23 September 2021, <https://astrobiology.nasa.gov/missions/kepler/>.

Way, MJ, Del Genio, AD, Kiang, NY, Sohl, LE, Grinspoon, DH, Aleinov, I, Kelley, M & Clune, T 2016, 'Was Venus the First Habitable World of our Solar System?', Geophysical Research Letters, https://doi.org/10.1002/2016GL069790>.

Williams, DR 2019, *Planetary Fact Sheet*, NASA, viewed 24 September 2021, <https://nssdc.gsfc.nasa.gov/planetary/factsheet/>.

Williams, M 2017, *What is the Radial Velocity Method*, Universe Today, viewed 30 March 2022, <https://www.universetoday.com/138014/radial-velocity-method/>.

Wilson, CF, Widemann, T & Ghail, R 2021, 'Venus: key to understanding the evolution of terrestrial planets', *Experimental Astronomy*, viewed 23 September 2021, <https://doi.org/10.1007/s10686-021-09766-0>.

Wilson, OC 1978, 'Chromospheric Variations in Main-Sequence Stars', *The Astrophysical Journal*, vol. 226, pp. 379-96, viewed 24 September 2021, <http://articles.adsabs.harvard.edu/pdf/1978ApJ...226..379W>.

Wordsworth, RD & Pierrehumbert, RT 2012, 'Water Loss from Terrestrial Planets with CO-$_2$-Rich Atmospheres', *The Astrophysical Journal*, vol. 778, no. 2, p. 19, viewed 24 September 2021, <https://doi.org/10.1088/0004-637X/778/2/154>.

Wright, JT 2018, 'Radial Velocities as an Exoplanet Discovery Method', in HJ Deeg & JA Belmonte (eds), *Handbook of Exoplanets*, Springer, Cham, ch Handbook of Exoplanets, pp. 619-31, viewed 30 March 2022, <https://link.springer.com/referenceworkentry/10.1007/978-3-319-55333-7_4?noAccess=true>.

Wright, JT & Gaudi, BS 2013, 'Exoplanet Detection Methods', *Springer*, pp. 489-540, viewed 23 September 2021, <https://doi.org/10.1007/978-94-007-5606-9_10>.

Yaqoob, T 2011, *Exoplanets and Alien Solar Systems*, New Earth Labs, Baltimore, viewed 23 September 2021, <https://books.google.com.au/books?id=QhaEz5p0TccC&pg=PR4&lpg=PR4&dq=Yaqoob,+T+2011,+Exoplanets+and+alien+Solar+systems,+New+Earth+Labs,+Baltimore&source=bl&ots=LLxRkKEwkJ&sig=ACfU3U1s7H8U64U1Kf7DBQxuBNv_wNbOZQ&hl=en&sa=X&ved=2ahUKEwjC2sXa9ZTzAhUGb30KHZyHBSgQ6AF6BAgMEAM#v=onepage&q=Yaqoob%2C%20T%202011%2C%20Exoplanets%20and%20alien%20Solar%20systems%2C%20New%20Earth%20Labs%2C%20Baltimore&f=false>.

Zhang, M, Yayaati, C, Kempton, EMR & Knutson, H 2019, 'Forward Modeling and Retrievals with PLATON, a Fast Open-source Tool', *Publications of the Astronomical*

Society of the Pacific, vol. 131, no. 997, <https://iopscience.iop.org/article/10.1088/1538-3873/aaf5ad>.

Zhang, M, Chachan, Y, Kempton, EMR, Knutson, HA & Chang, W 2020, 'PLATON II: NEW CAPABILITIES AND A COMPREHENSIVE RETRIEVAL ON HD 189733B TRANSIT AND ECLIPSE DATA', viewed 30 March 2022, <https://iopscience.iop.org/article/10.3847/1538-4357/aba1e6>.

APPENDIX

APPENDIX A: SPECIFICATIONS OF MAC OPERATING SYSTEM (OS) LAPTOP

OS Version: *macOS Catalina Version 10.15.7*

Processor: 2.9 GHz Dual-Core Intel Core i5

Memory: 8GB

Graphics: Intel Iris Graphics 6100 1536 MB

APPENDIX B: OVERVIEW OF THE INSTALLATION OF SIMULATION PROGRAMS

B.1: Installation of PLATON

PLATON is installed through the Mac terminal as per the PLATON installation information (Zhang et al. 2019). For this project, PLATON was downloaded from the GitHub repository (Zhang et al. 2020). The following line is used to download PLATON through the terminal:

```
>>git clone https://github.com/ideasrule/platon.git
>>cd platon/
>>python setup.py install
```

To test that the code is working, run the following line in the terminal:

```
>>nosetests -v
```

B.2: Installation of TauREx

TauREx III is installed through the Mac terminalas per the TauREx installation information (Al-Refaie et al. 2021). To install TauREx through the terminal, use the following commands:

```
>> pip install taurex
```

To test that the code is working, run a test:

```
>> python -c "import taurex; print(taurex.__version__)"
```

The following command is used to test that TauREx is working:

```
>> taurex
```

The command should run with no errors if the program has been installed correctly.

APPENDIX C: EXERTS OF CODE FROM SIMULATION PROGRAMS

C.1: Exert of code for PLATON

Note: *For this project, only the TransitDepthCalculator in PLATON will be used to model the transmission spectra of exoplanets.*

The following code is an example of the TransitDepthCalculator. This file can be downloaded from the PLATON GitHub repository (Zhang et al. 2020). By running this code, it will output a .dat file containing the wavelength (μm) and transit depth ($(R_S/R_P)^2$).

```
>>import numpy as np
>>import matplotlib.pyplot as plt
>>from platon.transit_depth_calculator import TransitDepthCalculator
>>from platon.constants import M_jup, R_sun, R_jup


>># All quantities in SI units:
>>Rs = 1.16 * R_sun                    #Radius of star
>>Mp = 0.73 * M_jup                    #Mass of planet
>>Rp = 1.40 * R_jup                    #Radius of planet
>>T = 1200          #Temperature of isothermal part of the atmosphere


>>#Create a TransitDepthCalculator object and compute wavelength dependent transit depths:
>>depth_calculator = TransitDepthCalculator(method="ktables") #put "xsec" for opacity sampling
>>wavelengths, transit_depths = depth_calculator.compute_depths(
   Rs, Mp, Rp, T, CO_ratio=0.2, cloudtop_pressure=1e4)

>>print("#Wavelength(m)      Depth")
>>for i in range(len(wavelengths)):
>>print(wavelengths[i], transit_depths[i])
```

```
>>plt.semilogx(1e6*wavelengths, transit_depths)
>>plt.xlabel("Wavelength (um)")
>>plt.ylabel("Transit depth")
>>plt.show()
```

In order for the output of PLATON to be used in TauREx, the inflated standard error needed to be calculated. This is because TauREx requires a 3-4 column ASCII format to read in the data. This file needs to be a .dat extension. The standard error was calculated using the in-built standard error function from SciPy (The SciPy community 2022). To inflate the standard error, the standard deviation was multiplied by two as per Tsiaras et al. (2021) which resulted in two times the standard error as per section 4.3.

The example code for the TransitDepthCalculator was modified as follows to be used as an input for TauREx:

```
>>import numpy as np
>>from numpy import histogram2d
>>import matplotlib.pyplot as plt
>>import pickle
>>import pandas as pd
>>From scipy.stats import sem
>>import math
>>from platon.transit_depth_calculator import TransitDepthCalculator
>>from platon.constants import M_jup, R_sun, R_jup, METRES_TO_UM
```

```
>># All quantities in SI
>>Rs = R_sun     #Radius of star
>>Mp = 4.867e+25     #Mass of planet
>>Rp = 6.0518e+6     #Radius of planet
>>T = 260           #Temperature of isothermal part of the atmosphere
>>T_star = 5778


>>#create a TransitDepthCalculator object and compute wavelength dependent transit depths:
depth_calculator = TransitDepthCalculator(method="xsec") #put "xsec" for opacity sampling:
>>wavelengths, transit_depths = depth_calculator.compute_depths(
   Rs, Mp, Rp, T, logZ=0.012, CO_ratio=0.5, T_star=T_star)


>># Convert wavelength from m to um for TauREx input
>>wavelengths = wavelengths * METRES_TO_UM


>># ADDED CODE
>># Determine standard error and create an array
>>stderror = sem(transit_depths)*2
>>stderror_array = np.empty([len(wavelengths)])
>>stderror_array.fill(stderror)
>>print(stderror_array)


>># Print wavelegnth, depth and error into table
>>print("#Wavelength(um)      Depth              Error")
>>for i in range(len(wavelengths)):
>>DataOut = print(wavelengths[i], transit_depths[i], stderror_array[i])


>># Save data as .dat file
>>DataOut = np.column_stack((wavelengths,transit_depths,stderror_array))
>>np.savetxt('venus.dat', DataOut, delimiter=" ")
```

```
>>print(DataOut)

>># Plot Transit Depth against Wavelength
>>plt.title("Venus")
>>plt.xscale("log")
>>plt.xlabel("Wavelength (um)")
>>plt.yscale("log")
>>plt.ylabel("(Rp/Rs)^2")
>>plt.errorbar(wavelengths, transit_depths, yerr=stderror_array)
>>plt.savefig("venus.jpg", dpi=200, bbox_inches="tight")
```

This will then output an ASCII table in a .dat format where the table reads (from left to right) the wavelength, transit depth and standard error for 461 values. This value is set as the default by PLATON.

PLATON will then output a plot of the transmission absorption spectrum of the exoplanet (see Figure 11).

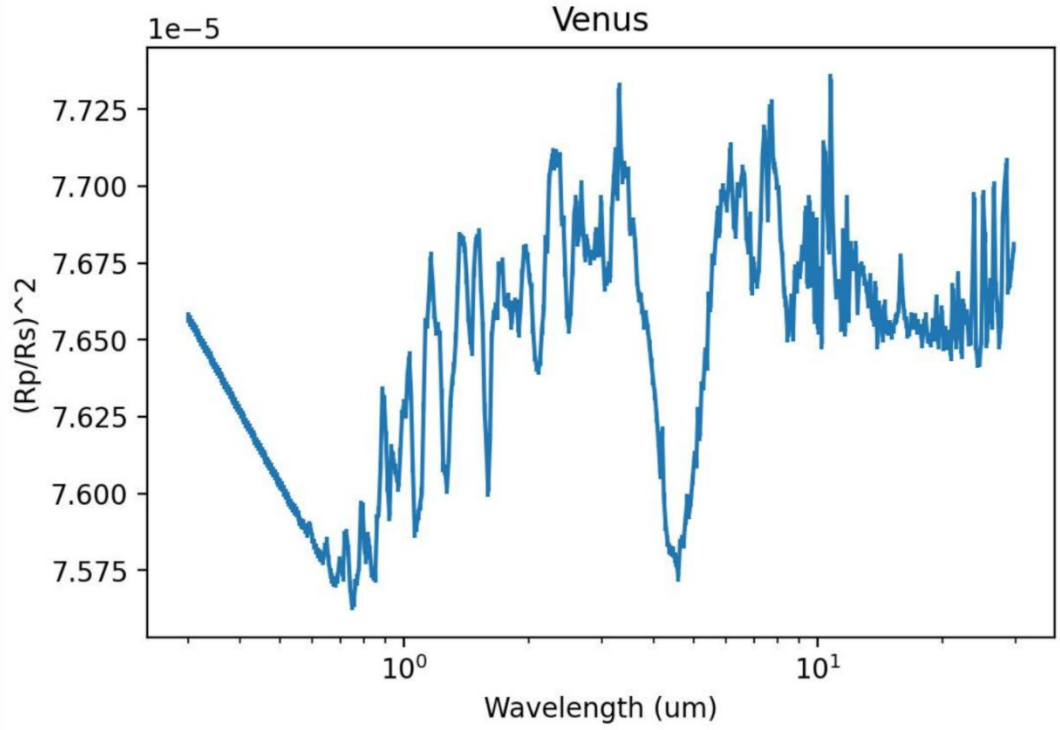

Figure 15: Example PLATON output of the transmission absorption spectrum of Venus. The x-axis represents the wavelength in microns (μm) as a logarithmic scale, and the y-axis represents the transit depth $((R_p/R_s)^2) \times 10^{-5}$.

C.2: Exert of code for TauREx

A .par file is used to specify the parameters of the star and exoplanet. This includes the exoplanets astrophysical parameters and its atmospheric composition. This is also where the user will specify the path for xsec (cross-section) and cia (collision-induced absorption) files required to model the data. These files are downloaded with the installation of TauREx. The paths are set under the heading [Global]:

```
>>[Global]
>> xsec_path = C:\path\to\xsec_files
```

The [Temperature] heading is used to set the temperature profile of the modelled planet in K. For this project, the profile_type was set to isothermal. Other options for this parameter can be found in the TauREx documentation:

>>[Temperature]
>>profile_type = isothermal
>>T = 230

The [Pressure] heading is used to set the pressure profile of the modelled planet. This heading allows the user to set the pressure at the top of the atmosphere (atm_max_pressure) and at the bottom of the atmosphere (atm_min_pressure) in Pa for a particular number of layers (n_layers). For this project, the profile_type was set to simple and the default pressure range for 100 layers. Other options for this parameter can be found in the TauREx documentation:

>>[Pressure]
>>profile_type = simple
>>atm_min_pressure = 1e0
>>atm_max_pressure = 1e6
>>n_layers = 100

The [Chemistry] heading of the .par file defines the molecular abundance in the planet atmosphere. For this project, the chemistry_type is set to taurex however, there are other options for this variable listed in the TauREx documentation (Al-Refaie et al. 2021). The fill_gases are gases used to fill the atmosphere. The ratio used for this is the abundance of the first listed molecule between the second listed molecule. The mix_ratio gases are set to an independent abundance value. Note that

the abundance is in decimal format. The total value of mix_ratio gases must be less than one, but not necessarily equal to one. This is because the TauREx code calculates the remainder of the fraction of molecular species to equal one. This is shown in the example code used in Al-Refaie et al. (2021). The user must also set the gas_type variable. For this project, this is set to constant. Other options for this variable are listed in the TauREx documentation (Al-Refaie et al. 2021).

Below is an example .par file using the [Chemistry] heading to define the molecular abundance of molecules in the modern Venus atmosphere which contains the active molecules CO_2, SO_2, H_2O and CO, and the inactive molecules He and N_2. In this project, the fill gas was used as a ratio of CO_2 to N_2 (CO_2:N_2):

```
>>[Chemistry]
>>chemistry_type = taurex
>>fill_gases = CO2, N2
>>ratio = 0.0363
>>
>>      [[SO2]]
>>      gas_type = constant
>>      mix_ratio = 0.00015
>>
>>      [[H2O]]
>>      gas_type = constant
>>      mix_ratio = 0.00002
>>
>>      [[CO]]
>>      gas_type = constant
>>      mix_ratio = 0.000017
```

>>

>>	[[He]]

>>	gas_type = constant

>>	mix_ratio = 0.000012

The [Planet] heading is used to define the astrophysical parameters of the planet. This includes the planet mass in M_{Jup}, the planet radius in R_{Jup}, the planet distance in au, and the orbital period in days. For this project, the planet_type was set to simple. Other options for this variable can be found in the TauREx documentation (Al-Refaie et al. 2021). Below is an example of the parameters used for the Venus model in TauREx:

>>[Planet]

>>planet_type = Simple

>>planet_mass = 2.565e-3

>>planet_radius = 8.4e-2

>>planet_distance = 0.723

>>orbital_period = 225

Like the [Planet] heading, the [Star] heading is used to define the parameters of the star such as its temperature in K. For this project, the star_type was set to blackbody. Other options for this variable can be found in the TauREx documents (Al-Refaie et al. 2021):

>>[Star]

>>star_type = blackbody

>>temperature = 5778

The [Model] heading is used to set the type of model outputted by TauREx. For this project, a transmission absorption spectrum with Rayleigh Scattering contributions was outputted. Other parameters available for the [Model] heading can be found in the TauREx documentation (Al-Refaie et al. 2021):

```
>>[Model]
>>model_type = transmission
>>      [[Absorption]]
>>      [[Rayleigh]]
```

The [Observation] heading allows users to input observation data from an external source. For this project, the data used was in the format of a 3-column ASCII .dat file. The observation data is inputted into TauREx by setting the path to the file:

```
>>[Observation]
>>observed_spectrum = /path/to/observation_data_file/
```

The .par file can then be run in the terminal, using the following command:

```
>>taurex -I filename.par –plot
```

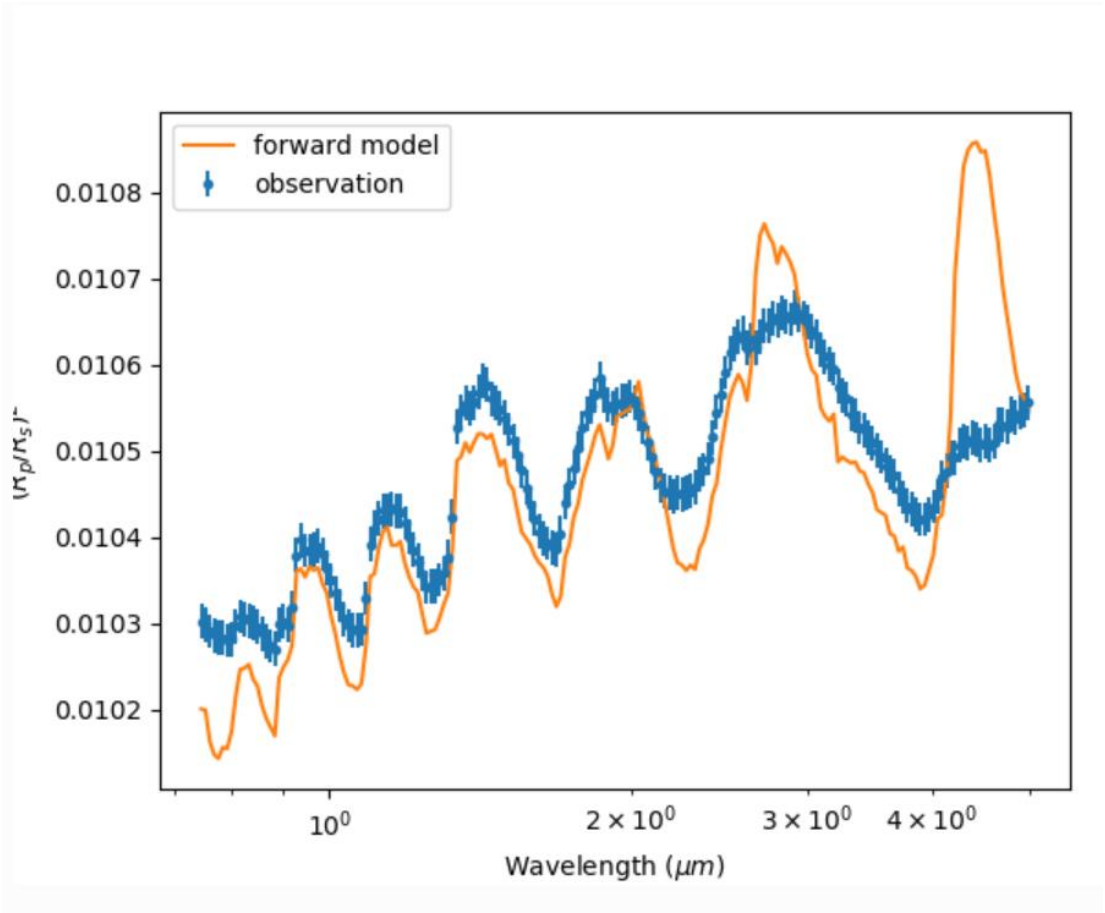

Figure 16: Example output of a transmission absorption spectral model and observations in TauREx. The x-axis represents the wavelength in microns (µm) as a logarithmic scale, and the y-axis represents the transit depth ($(R_p/R_s)^2$). Sourced from Al-Refaie et al. (2021).

This command outputs the forward model. If an observation data file path is set in the .par, TauREx will output the model and the data as one plot. An example of this is shown in Figure 12.

A plot of the molecular contributions to the spectrum can also be outputted (see Figure 13). To do this, the following command is run in the terminal:

>> taurex -I filename.par –plot -C

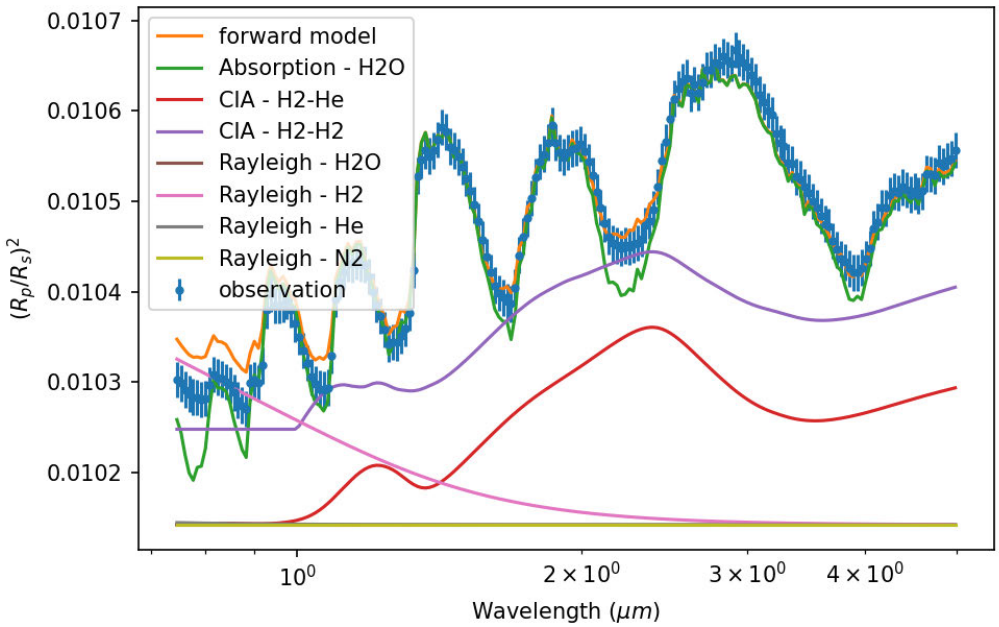

Figure 17: Example output of a transmission absorption spectral model, observation and the molecular contributions in TauREx. The x-axis represents the wavelength in microns (µm) as a logarithmic scale, and the y-axis represents the transit depth ($(R_p/R_s)^2$). Sourced from Al-Refaie et al. (2021).